Eur. Phys. J. C (2017) 77:120
DOI 10.1140/epjc/s10052-017-4656-5

THE EUROPEAN PHYSICAL JOURNAL C

Regular Article - Theoretical Physics

Scattering of W and Z bosons at high-energy lepton colliders

Christian Fleper[1,a], **Wolfgang Kilian**[1,b], **Jürgen Reuter**[2,c], **Marco Sekulla**[3,d]

[1] Department of Physics, University of Siegen, 57068 Siegen, Germany
[2] DESY Theory Group, 22607 Hamburg, Germany
[3] Institute for Theoretical Physics, Karlsruhe Institute of Technology, 76128 Karlsruhe, Germany

Received: 5 August 2016 / Accepted: 30 January 2017 / Published online: 22 February 2017

Abstract We present a new study of quasi-elastic W and Z scattering processes in high-energy e^+e^- collisions, based on and extrapolating the low-energy effective theory which extends the standard model with a 125 GeV Higgs boson. We parameterize deviations in the low-energy range in terms of the dimension-eight operators that arise in the effective theory. Smoothly extending this to higher energy, we study a set of simplified models of new physics in W/Z scattering, (1) a structureless extrapolation of the effective theory, and (2) scalar and tensor resonance multiplets. The high-energy asymptotics of all models is regulated by a universal unitarization procedure. This enables us to provide benchmark scenarios which can be meaningfully evaluated off shell and in exclusive event samples, and to determine the sensitivity of an e^+e^- collider to the model parameters. We analyze the longitudinal vector-boson scattering modes, where we optimize the cuts for the fiducial cross section for different collider scenarios. Here, we choose energy stages of 1.0, 1.4 and 3 TeV, as motivated by the extendability of the ILC project and the staging scenario of the CLIC project.

1 Introduction

Quasi-elastic scattering processes of the massive electroweak bosons $W^\pm$, Z (vector-boson scattering, VBS) are a cornerstone in the phenomenology of electroweak interactions. The longitudinal polarization components of on-shell energetic W and Z particles are closely related to the unobservable Goldstone bosons that constitute the elementary Higgs doublet together with the physical Higgs boson [1,2]. Their interactions thus probe the mechanism of electroweak symmetry breaking.

If the Higgs was missing from the particle spectrum, the W/Z interaction strength would rise with energy into a non-perturbative regime, indicating an intrinsic cutoff of the effective theory and new strong interactions [3,4]. However, the recent discovery of a 125 GeV Higgs boson implies that this is not the case. The existence of the Higgs boson allows all VBS interactions to remain weak asymptotically, calculable in electroweak perturbation theory. For the necessary cancelation of terms to take effect to all orders, the vector-boson, Higgs and Goldstone couplings must coincide exactly with their standard model (SM) values [5].

Without sufficient experimental data, we cannot decide whether the pure SM is the correct description of the electroweak symmetry-breaking sector. Beyond the SM, processes that involve Higgs and Goldstone fields could rather open a new portal to phenomena and structures that do not couple directly to matter particles, and they are thus detached from immediate experimental access. Collider experiments will have to search for new effects in this area and complete our knowledge about the particle and interaction spectrum at accessible energies.

VBS processes have been observed at the large hadron collider (LHC) in Run I [6–8], and the analysis of future LHC runs at full energy and increased luminosity will considerably improve our knowledge in this sector. At hadron colliders, VBS is accessible in processes of the type $pp \to q^*q^* \to qq + VV$, where q indicates any light quark, and $V = W, Z$. The analysis has been demonstrated to be feasible, but nevertheless suffers from limitations that do not simply disappear with increasing collider luminosity or energy. Leptonic decays of vector bosons either yield incomplete kinematic information (W) or a low branching ratio (Z). Hadronic decays are difficult to isolate from a large QCD background. VBS processes must be separated from vector-boson pair production, $q\bar{q}' \to VV$, QCD production of VV

[a] e-mail: christian.fleper@uni-siegen.de
[b] e-mail: kilian@physik.uni-siegen.de
[c] e-mail: juergen.reuter@desy.de
[d] e-mail: marco.sekulla@kit.edu

and two jets, as well as top-quark production as SM background. The initial state, i.e., the flavor and energy of the initial quarks, cannot be controlled or detected, and steeply falling parton structure functions limit the accessible energy for the elementary VBS interaction.

By contrast, e^+e^- colliders provide a clean environment where the VBS process class has a unique signature, and most decays of W and Z bosons are accessible and can be observed with high efficiency and purity [9,10]. The initial state is known exactly, and the e^+e^- c.m. energy is fixed up to minor electromagnetic radiation effects. We expect more detailed and complementary information to be available from e^+e^- collisions compared to hadronic collisions. The decisive factor for an e^+e^- collider is the availability of sufficient energy combined with high luminosity.

The complete list of e^+e^- VBS processes accessible at an e^+e^- collider with sufficient energy reads

$$e^+e^- \to \bar{\nu}_e \nu_e W^+W^-, \tag{1}$$
$$\bar{\nu}_e \nu_e ZZ, \tag{2}$$
$$\bar{\nu}_e e^- W^+ Z, \tag{3}$$
$$e^+ \nu_e Z W^-, \tag{4}$$
$$e^+e^- W^+W^-, \tag{5}$$
$$e^+e^- ZZ \tag{6}$$

with various decay channels of the final-state bosons. These processes allow us to study interactions of W and Z bosons in the following elementary scattering channels, which are realized as distinct, approximately on-shell factorized contributions to the amplitudes:

$$W^+W^- \to W^+W^-, \tag{7}$$
$$W^+W^- \to ZZ, \tag{8}$$
$$W^\pm Z \to W^\pm Z, \tag{9}$$
$$ZZ \to W^+W^-, \tag{10}$$
$$ZZ \to ZZ. \tag{11}$$

By kinematics alone, the threshold for these processes is just above the vector-boson pair production threshold of 160 . . . 180 GeV, but for a meaningful analysis of deviations from the SM, a significantly larger vector-boson pair energy (i.e., invariant mass of the VV system) is necessary.

The prospects for the measurement of VBS processes at lepton colliders, including potential non-SM contributions, have been studied extensively in the literature [11–21]. However, most previous studies have investigated no-Higgs (or heavy-Higgs) scenarios, occasionally in comparison to the pure SM with a light Higgs of some arbitrarily assumed mass. Since a Higgs-like boson has been found, its mass has been precisely determined, and the measurement of its couplings is in accordance with the pure SM prediction, Higgs-less models do no longer provide a viable scenario for electroweak interactions. The analysis of VBS should rather be based on models that reduce to the SM with a 125 GeV Higgs at low energy and take into account all recently accumulated knowledge about the Higgs boson.[1]

In this paper, we therefore present a new study of VBS processes at an e^+e^- lepton collider. We take the SM with a Higgs mass of 125 GeV as reference and determine the sensitivity to effects beyond the SM in VBS interactions. Given the exploratory nature of this task and the emergence of strong-interaction effects, we can restrict our calculation to leading order in the SM and EFT predictions. Actual data analysis should incorporate NLO corrections in the SM and its EFT extension, cf. [23–25], which eventually should become available for the complete six-fermion partonic processes.

If the EFT is extrapolated to high energy, for nonzero higher-dimension operator coefficients the calculated amplitudes inevitably enter a regime where partial-wave unitarity becomes an issue, i.e., the model becomes strongly interacting. It is meaningless to use the perturbative and truncated EFT expansion unmodified within and beyond this range. Any model must satisfy the following two constraints: (1) at low energy, it reduces to the low-energy EFT, and (2) for all energies, it should be in accordance with quantum-mechanical unitarity.

In the present work, we realize this program by starting with seed models that either naively continue the EFT without new structure, or include new particle states with arbitrary mass and coupling and thus extra free parameters. For each of these seed models, we apply a universal unitarization method, the T-matrix framework. The thereby generated models are unitary by construction and thus satisfy both of the above constraints. Furthermore, they provide a range of distinct asymptotical behavior that should be sufficient for an initial phenomenological analysis in a range where data will be difficult to obtain.

The concrete results are computed for specific values of the collider energy, $\sqrt{s} = 1.4$ and 3.0 TeV with integrated luminosities of $\mathcal{L}_{\text{int}} = 1.5$ and 2 ab^{-1}, as planned for the Compact Linear Collider (CLIC) [26–28]. Furthermore, we make use of specific properties of the CLIC collider environment in its currently planned state, including the most relevant detector properties, to estimate the sensitivity on anomalous effects beyond the SM. For completeness, we also include numbers for a lower collider energy of 1 TeV with an integrated luminosity of $\mathcal{L}_{\text{int}} = 5$ ab^{-1}, which should also illuminate the potential of an energy upgrade of the international linear collider (ILC) [29,30].

[1] Turning this around, VBS at high energy can be utilized to supply indirect information on Higgs boson properties [22].

2 Effective field theory and vector-boson scattering

The theoretical basis for the current study is the SM with a single complex Higgs doublet. Since we want to provide not just the unique SM prediction but a range of possibilities for the high-energy behavior of electroweak interactions, we have to regard the SM as an effective field theory (EFT). I.e., we assume an infinite series of interactions, organized by operator dimension [31–33]. The pure SM limit consists of setting the couplings of all operators with dimension greater than four to zero, or alternatively, letting the intrinsic mass scale of those dimensionful couplings to infinity.

Within the EFT formalism, we assume that the strong–electroweak $SU(3)_{\rm QCD} \times SU(2)_L \times U(1)_Y$ gauge symmetry of the SM Lagrangian is a fundamental property, and therefore organize all higher-dimensional operators in terms of gauge-invariant polynomials. This implies global strong–electroweak invariance for all terms and promoting partial derivatives to covariant derivatives where required by the field representation. We do not consider CP symmetry-breaking effects (beyond those already present in the SM) in the current study.

The SM Higgs, in the gauge-invariant Lagrangian, appears as a complex doublet which transforms linearly under $SU(2)_L \times U(1)_Y$.[2] If we neglect the interactions of heavy SM fermions, the global symmetry is approximately $SU(2)_L \times SU(2)_R$ [35,36]. This symmetry is explicitly broken by the hypercharge gauge coupling. The obstruction can be controlled as a spurion, and the analysis can be based on an exactly $SU(2)_L \times SU(2)_R$ symmetric Lagrangian. This is a reasonable simplification since we are interested in the high-energy range of VBS processes where gauge interactions play a minor role, i.e., can be viewed as a perturbation entirely. The Higgs vacuum expectation value (vev) spontaneously breaks the global symmetry down to the diagonal $SU(2)_{L+R}$, known as the custodial symmetry $SU(2)_C$.

In this context, it is natural to represent the Higgs field multiplet as a 2×2 matrix [37,38],

$$\mathbf{H} = \frac{1}{2}\begin{pmatrix} v + h - \mathrm{i}w^3 & -\mathrm{i}\sqrt{2}w^+ \\ -\mathrm{i}\sqrt{2}w^- & v + h + \mathrm{i}w^3 \end{pmatrix}. \tag{12}$$

which transforms linearly under $U \in SU(2)_L$ and $V \in SU(2)_R$ as

$$\mathbf{H} \to U\mathbf{H}V^\dagger. \tag{13}$$

[2] A non-linear Higgs representation might be chosen to allow for more freedom in Higgs couplings that are not yet constrained with precision, but this property is of secondary importance in our study of VBS processes. It becomes more relevant when considering also Higgs final states, cf. [34].

The covariant derivative of the Higgs matrix is given by

$$\mathbf{D}_\mu \mathbf{H} = \partial_\mu \mathbf{H} - ig\mathbf{W}_\mu \mathbf{H} + ig'\mathbf{H}\mathbf{B}_\mu \tag{14}$$

where

$$\mathbf{W}_\mu \equiv W_\mu^a \frac{\tau^a}{2}, \quad \mathbf{B}_\mu \equiv B_\mu \frac{\mathbf{T}}{2} \tag{15}$$

and $\mathbf{T}$ is a $SU(2)_R$-breaking spurion with ground state $\mathbf{T} = \tau^3$. Finally, we define the matrix-valued field strengths

$$\mathbf{W}^{\mu\nu} = \partial_\mu \mathbf{W}_\nu - \partial_\nu \mathbf{W}_\mu - \mathrm{i}g\left[\mathbf{W}_\mu, \mathbf{W}_\nu\right], \tag{16}$$

$$\mathbf{B}^{\mu\nu} = \partial_\mu \mathbf{B}_\nu - \partial_\nu \mathbf{B}_\mu \tag{17}$$

and quote the bosonic part of the SM Lagrangian (omitting QCD),

$$\begin{aligned} \mathcal{L}_{SM} = &-\frac{1}{2}\,\mathrm{tr}\left[\mathbf{W}_{\mu\nu}\mathbf{W}^{\mu\nu}\right] - \frac{1}{2}\,\mathrm{tr}\left[\mathbf{B}_{\mu\nu}\mathbf{B}^{\mu\nu}\right] \\ &+ \mathrm{tr}\left[\left(\mathbf{D}_\mu \mathbf{H}\right)^\dagger \mathbf{D}^\mu \mathbf{H}\right] \\ &+ \mu^2\,\mathrm{tr}\left[\mathbf{H}^\dagger\mathbf{H}\right] - \frac{\lambda}{2}\left(\mathrm{tr}\left[\mathbf{H}^\dagger\mathbf{H}\right]\right)^2. \end{aligned} \tag{18}$$

The power of an EFT series as a perturbative expansion lies in the accuracy of a truncation at low order. New mutual and self-interactions of bosons only take the form of gauge-invariant operators of even dimension. The leading non-SM order is thus dimension six, so it appears natural to truncate the EFT at this order. The complete set of dimension-six operators has been discussed extensively in the literature [39–44].

However, new-physics effects in the Higgs–Goldstone sector, including new strong interactions, largely decouple from precision observables as they are accessible today. While several dimension-six operators in the EFT do affect VBS processes at tree level, they simultaneously modify other couplings which can be measured independently. Such operators are an inadequate representation of the specific new-physics scenarios that VBS is most sensitive to. In fact, for the purpose of studying VBS, we may assume that the coefficients of dimension-six operators are known to sufficient precision; we set them to zero as the standard reference point.

Traces of genuine new Higgs–Goldstone physics appear first in dimension-eight operators. These modify VBS interactions independently of other types of interaction. For instance, the exchange of massive resonances generically results in dimension-eight effective operators [45]. Our study therefore includes the relevant dimension-eight operators.

It is evident that any truncation at this level, while technically consistent, is of questionable value. Amplitudes modified by dimension-eight operators rise rapidly with energy

and thus yield large effects [38]. This fact also indicates the breakdown of the perturbative expansion. An extrapolation of the low-energy EFT with dimension-eight operators can therefore not be understood as an approximation that can be systematically improved. It rather serves as a phenomenological tool to parameterize dominant non-SM phenomena in VBS. At low energy, $O(100\ \text{GeV})$, it smoothly matches to the EFT within its range of validity. Extrapolated to high energy, it becomes a two-parameter simplified model which exhibits BSM effects in form of a strongly interacting continuum. The extrapolation incorporates unitarity as the only damping mechanism and thus asymptotically approaches the unitarity bound for each partial-wave amplitude. However, additional structure can easily be included, as we will describe below using alternative simplified models containing resonances.

3 Anomalous interactions of vector bosons

The complete set of dimension-eight operators for the SM fields is rather large. In line with the above considerations, we resort to standard simplifications in order to make the set manageable. First of all, as stated before, we only consider bosonic operators. (That is, we treat fermionic currents as external probes for bosonic interactions, neglecting genuine fermionic anomalous contributions.) We furthermore assume the global $SU(2)_L \times SU(2)_R$ symmetry of the fermion- and gaugeless SM to hold also at higher orders. This introduces relations between W and Z scattering amplitudes and simplifies the scattering matrix for the purpose of unitary extrapolation.

Focusing on operators that directly modify quartic vector-boson interactions, there are three classes which affect Higgs/Goldstone bosons only (index: S), gauge bosons only (index: T), or both (index: M), respectively. We recall that, taking EWSB into account, Goldstone bosons are probed via the longitudinal polarization direction of energetic W and Z bosons, while gauge bosons translate into transversal polarization.

Operators involving only the Higgs/Goldstone-boson sector, i.e., S-type, are represented by a combination of covariant derivatives acting on the Higgs fields. Two linearly independent operators can be identified

$$\mathcal{L}_{S,0} = F_{S,0}\,\mathrm{tr}\left[\left(\mathbf{D}_\mu \mathbf{H}\right)^\dagger \mathbf{D}_\nu \mathbf{H}\right]\mathrm{tr}\left[\left(\mathbf{D}^\mu \mathbf{H}\right)^\dagger \mathbf{D}^\nu \mathbf{H}\right], \tag{19a}$$

$$\mathcal{L}_{S,1} = F_{S,1}\,\mathrm{tr}\left[\left(\mathbf{D}_\mu \mathbf{H}\right)^\dagger \mathbf{D}^\mu \mathbf{H}\right]\mathrm{tr}\left[\left(\mathbf{D}_\nu \mathbf{H}\right)^\dagger \mathbf{D}^\nu \mathbf{H}\right]. \tag{19b}$$

In the present paper, we do not study the transversal and mixed interactions but defer this to future work. For completeness, we list the T and M-type operators in the appendix. We also neglect operators which are proportional to $\mathbf{H}^\dagger\mathbf{H}$; as long as Higgs final states are not considered, this class of operators merely renormalizes the dimension-six part of the EFT Lagrangian.

We may compare this EFT framework with the corresponding expansion [46,47] and subsequent analysis for the no-Higgs (or heavy-Higgs) case, as it was investigated, for instance, in [17,18]. In the pure SM, a light Higgs boson and no higher-order operators, the amplitude for VBS remains perturbative at all energies. Beyond the SM, new physics that appears exclusively in the Higgs–Goldstone sector corresponds to dimension-eight operators as argued above, therefore any deviation from the SM increases rapidly with energy. Since the pure SM amplitude is small, interference plays a minor role and the phenomenologically relevant behavior originates from the dimension-eight interactions, squared. By contrast, if the light Higgs boson did not exist, the reference amplitude would grow with energy and render the interaction strong in the TeV range by itself, while anomalous effects would contribute first via their interference, which is a less striking modification of the reference amplitude. In this study, which is based on the now established light-Higgs scenario, we therefore will face a sudden transition from a weakly interacting to a strongly interacting regime when increasing the energy in the VBS process.

4 Unitary extrapolation

The SM amplitudes for VBS, as for any other elementary process, are perturbative throughout the accessible energy range and therefore do not pose a unitarity problem. If anomalous effects are present which cannot simply be mapped to an extended renormalizable (weakly interacting) model, this property is lost, and we have to deal with unitarity violation in the tree-level prediction. Clearly, this indicates the breakdown of perturbation theory and of the EFT paradigm. On the other hand, the quantitative analysis of actual data relies on the availability of a prediction which depends on a suitable set of new parameters. Such a reference allows us to quantitatively study or exclude a deviation from the SM. In order to discard grossly unphysical parameterizations, we have to ensure that any such extrapolation is at least in accordance with unitarity, all assumed symmetries, and smoothly matches to the low-energy effective theory.

In [38,48], based on earlier work in [49], we have described the T-matrix unitarization framework as a generic scheme that allows for a unitary extrapolation of any model without introducing arbitrary artifacts in the asymptotic regime. We adopt this framework for the current paper.

At the fundamental level of the complete scattering matrix $\mathbf{S} = 1 + \mathrm{i}\mathbf{T}$ (T-matrix), the unitarization framework relies on the formula

$$\mathbf{T}(\mathbf{T}_0) = \frac{1}{\mathrm{Re}\left(\mathbf{T}_0{}^{-1}\right) - \frac{\mathrm{i}}{2}\mathbb{1}}\,, \tag{20}$$

which transforms an arbitrary model of the scattering matrix $\mathbf{T}_0$ into a unitary model of the scattering matrix $\mathbf{T}$. In particular, the set of amplitudes is invariant under the transformation if it already respects unitarity. For the application of the formula, it is advantageous to diagonalize the scattering matrix first and apply unitarization to eigenamplitudes, since this amounts to a simple multiplication or subtraction. In the present context, this can be done most easily in the high-energy limit where the gauge sector decouples from the Higgs sector. Since unitarity is an issue only for high energies, such an approach is sufficient to remove all dangerous terms.

The method does not refer to any property of the original model which is encoded in $\mathbf{T}_0$; in particular, it does not assume a perturbative expansion or a particular analytical structure. While it reconciles any model $\mathbf{T}_0$ with unitarity, the result is not a unique prediction. It is merely a model that describes possible behavior of the amplitude up to the highest energies, as opposed to a unitarity-violating model or extrapolation that describes impossible behavior.

In practice, we identify the asymptotically leading terms in the diagonal scattering matrix, replace them by their unitary equivalents, and invert the diagonalization. Factoring out Lorentz tensors and subtracting the original EFT contribution, we cast this in the form of extra momentum-dependent Feynman rules. The new terms resemble the local Feynman rules that describe the original EFT operators, but they carry prefactors that depend on invariant momentum combinations in a non-analytical form. Nevertheless, for calculational purposes the new terms play a role analogous to the local counterterms that arise in a NLO calculation, and they are straightforward to take into account in the construction and evaluation of scattering matrix elements. This allows us to perform off-shell calculations and evaluate the unitarized amplitudes for external fermions, as long as the kinematic assumptions underlying the procedure are satisfied.

For illustration, in plots below (Figs. 4, 5, 6) we display both the unitarized model behavior and the unphysical results that we would have obtained without unitarization. The latter are marked as dashed lines, while continuous curves refer to the respective unitary versions. While for some parameter sets, the unitarization correction remains a minor issue, there are various cases where unitarization has a large impact. This property clearly indicates that, for CLIC energies, VBS processes are probed in a range where undetermined new-physics effects are actually important, and systematic approximations do no longer yield unambiguous results. Under no circumstances, calculation results without unitarization may be used for the analysis of actual data, as this would grossly overestimate the sensitivity on the model parameters.

5 Cut-based extraction of the VBS signal

Based on the theoretical framework as described above, we now turn to the actual prospects for measuring vector-boson scattering processes at high effective energy at a high-energy lepton collider, like e.g. the CLIC collider. The strategy of such an analysis does not depend strongly on the underlying physics model. We can therefore follow the ideas of [13,17,18] and adapt the analysis to the CLIC environment.

For this parton-level study, we restrict ourselves to fully hadronic decays of the massive vector bosons which constitute the major part of the cross section. That is, we are considering all final states $4q+2f$, where each f may be either a (not necessarily detected) lepton or an invisible neutrino. As discussed already in [13], $qqgg, t\bar{t}$ production, and any other reducible backgrounds can be safely neglected after applying the cuts that we describe below. The important issue is to identify that part of the partonic event sample which actually depends on the physics of interest and enhance its contribution by a careful selection.

The main idea is to isolate a signal of vector-boson pairs in association with very forward neutrinos or electrons. This is the kinematic situation where in the diagrams of Fig. 1, the incoming vector bosons which participate in the VBS interaction have small invariant mass, so the amplitude is enhanced by the small denominator of the t-channel propagators. The nonvanishing mass of $V = W, Z$ bosons cuts off the approach to the actual particle pole, so the enhancement factor is of order m_V^2/E_V^2 in this kinematic range, and the typical recoil p_T of the radiating lepton becomes of order m_V. Graphs without the VBS interaction (Figs. 2, 3) do not benefit from this effect.

For identifying background-type regions, we first note that a large part of the total rate is due to W-boson pair production initiated by photons, cf. Fig. 3 (left). Photon-induced VBS processes are interesting by themselves, but photons

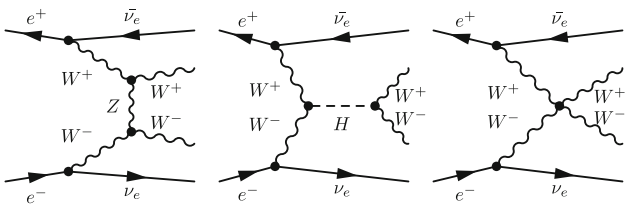

Fig. 1 Signal Feynman diagrams contributing to the VBS process

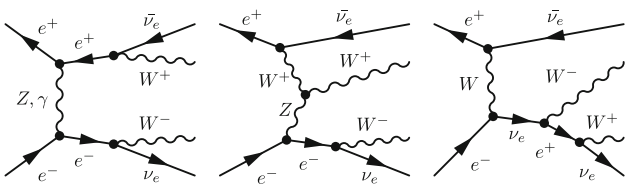

Fig. 2 Feynman diagrams contributing to the irreducible background

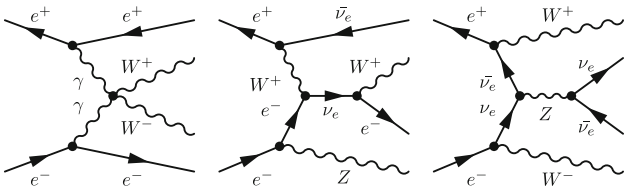

Fig. 3 Feynman diagrams contributing to the partially reducible background

do not have a longitudinal component and therefore do not receive contributions from new physics in the Higgs sector. For our purposes, the photon-induced contribution is therefore considered as a background. In contrast to the distribution of intermediate W/Z bosons, which is dominated by $Q \sim m_{W/Z}$, the distribution of photons extends down to nearly zero momentum transfer and is cut off only by the finite electron mass. Electrons in the forward direction disappear in the beampipe and are thus indistinguishable from neutrinos, so in this kinematic range, intermediate photons cannot be separated by detecting the radiating fermion. Nevertheless, this background can be reduced without losing too much of the signal by vetoing against very forward electrons and simultaneously cutting on the p_T distribution of the vector-boson pair system.

We are interested in the vector-boson pair system at large combined invariant mass, as this is the energy value that enters the basic VBS interaction. Hence, we propose the following set of selection cuts, where the first number always refers to the 3.0 TeV CLIC staging, while the one in parentheses corresponds to the lower-energy staging at 1.4 TeV.

1. $M_{\text{inv}}(\bar{\nu}\nu) > 230(175)$ GeV. The signal process contains two neutrinos in the final state. This cut removes events where the neutrinos originate from Z decay; a majority of these neutrinos will have an invariant mass $M_{\text{inv}}(\bar{\nu}\nu) \sim 91$ GeV. Backgrounds from W^+W^- and QCD four-jet production are also removed by this cut.
2. $|\cos\theta(W/Z)| < 0.8$ and $p_\perp(W/Z) > 300(180)$ GeV. Events where the vector bosons have a small distance from the beam pipe or a small transverse momentum are cut away. This reduces backgrounds which result from t-channel exchange in the subprocess.
3. $\theta(e) > 15$ mrad and $p_\perp(WW) > 100(50)$ GeV, $p_\perp\ (ZZ) > 60(40)$ GeV. Together with a cut on the transverse momentum of the vector-boson pair system, background resulting from $\gamma\gamma$ fusion will substantially be decreased.
4. 900(800) GeV $< M_{\text{inv}}(WW) <$ 1900(1175) GeV, 850(800) GeV $< M_{\text{inv}}(ZZ) <$ 1900(1175) GeV. The influence of the operators, see Eq. (19), increases with the invariant mass of the vector-boson pair. We therefore only consider events within a small invariant mass range.

The following cuts are applied for the ILC staging scenario at 1.0 TeV:

1. $M_{\text{inv}}(\bar{\nu}\nu) > 150$ GeV.
2. $|\cos\theta(W/Z)| < 0.8$ and $p_\perp(W/Z) > 150$ GeV.
3. $\theta(e) > 15$ mrad and $p_\perp(WW) > 45$ GeV, $p_\perp(ZZ) > 40$ GeV.
4. 575 GeV $< M_{\text{inv}}(WW) <$ 800 GeV, 600 GeV $< M_{\text{inv}}(ZZ) <$ 800 GeV.

For the calculation, we have used the implementation of the SM in the WHIZARD Monte-Carlo generator [50,51]. The SM extensions that we consider in later sections are likewise handled by dedicated WHIZARD model implementations, taking into account unitarization corrections where necessary. The WHIZARD generator provides a physics simulation framework that can include beam properties (polarization, beamstrahlung and ISR), the complete partonic final state to leading and next-to-leading order QCD, parton shower, and hadronization, eventually complemented by detector-level tools and analysis methods [52–59].

For this exploratory study, we have largely restricted ourselves to on-shell W/Z bosons in the final state and concentrate on total cross section values after cuts. Polarization, ISR, and beamstrahlung are not taken into account for the tables below. Further below, we comment on possible improvements if polarization and details of the partonic final state are taken into account, using off-shell simulation for the latter. We expect that a future experimental study which can be performed using the WHIZARD generator in connection with detector simulation, jet algorithms, etc., should give more accurate results which we nevertheless expect to lie in the numerical range as our final results suggest. Clearly, especially ISR and beamstrahlung will lead to a distortion of distributions and to a depletion of events in the high-energy region, but we do not expect our results to fundamentally change. Our first estimates which should be backed up by future experimental studies confirmed that, and especially the number that roughly half of the events is in the highest ten-percent energy bin from Table 2.2 in [26] when beamstrahlung is actually simulated.

Tables 1 and 2 contain our results for the SM cross sections of the processes of interest, before and after cuts, respectively. As argued above, the results apply to on-shell bosons in the final state and do not refer to detailed properties of the CLIC collider, with two notable exceptions that we discuss in the following.

1. For suppressing the contribution from photon-induced processes, the analysis has to rely on the ability to detect energetic electrons in the very forward region, which are barely deflected by the photon emission. If such electrons

Table 1 Standard model total cross sections in fb (±1% error) without cuts for center-of-mass energies of $\sqrt{s} = 1.4$ TeV and 3 TeV. Both particle beams are unpolarized. Detection efficiencies and branching ratios are not included. All cross sections have to be multiplied by the factors in the fourth column to take the misidentification of vector bosons into account

Process	1.4 TeV	3 TeV	Factor
$W^+W^-\nu\bar{\nu}$	47.1	132	1
$W^+W^-e^+e^-$	1570	3820	1
$W^\pm Ze^\mp\nu$	138	408	0.136
ZZe^+e^-	3.78	4.70	0.019
$W^+W^-(Z \to \nu\bar{\nu})$	11.7	9.35	1
$ZZ\nu\bar{\nu}$	15.7	57.5	1
ZZe^+e^-	3.78	4.70	1
$W^\pm Ze^\mp\nu$	138	408	0.136
$W^+W^-e^+e^-$	1570	3820	0.019
$ZZ(Z \to \nu\bar{\nu})$	0.484	0.237	1

Table 2 Same as Table 1, but with cuts

Process	1.4 TeV	3 TeV	Factor
$W^+W^-\nu\bar{\nu}$	0.119	0.790	1
$W^+W^-e^+e^-$	0.000	0.000	1
$W^\pm Ze^\mp\nu$	0.269	1.200	0.136
ZZe^+e^-	0.000	0.000	0.019
$W^+W^-(Z \to \nu\bar{\nu})$	0.039	0.610	1
$ZZ\nu\bar{\nu}$	0.084	0.790	1
ZZe^+e^-	0.000	0.000	1
$W^\pm Ze^\mp\nu$	0.288	1.590	0.136
$W^+W^-e^+e^-$	0.000	0.000	0.019
$ZZ(Z \to \nu\bar{\nu})$	0.000	0.000	1

are vetoed against, the ambiguity between W and Z/γ bosons in the initial state is greatly reduced. For the current study we have assumed that a veto against electrons is possible down to an angle of 15 mrad [60].

2. The clean environment and triggerless operation of a lepton collider allows us to detect final-state vector bosons by their decay products in essentially all channels. For the current study, we have concentrated on the hadronic decay channels. These decays provide the major part of the decay branching fractions and yield complete kinematic information. In particular, the momenta of the forward neutrinos can be inferred from the missing energy and momentum. A disadvantage of hadronic channels is the absence of charge information and the finite jet-pair invariant mass resolution, which adds on the natural decay width of W and Z bosons. As a result, there is a probability for misidentification between W and Z. We take this into account by the matrix for identification probabilities as it was determined in [61]:

$$W \to 88\%\ W,\ 12\%\ Z \tag{21a}$$
$$Z \to 12\%\ W,\ 88\%\ Z \tag{21b}$$

Partonic WW, WZ and ZZ final states therefore will be identified as a $WW(ZZ)$ event with probabilities 77.4, 10.6, 1.4%, which yields the weighting factors 1:0.136:0.019 given in the final column of both Tables 1 and 2. Taking the hadronic W and Z boson branching ratios of 67.70 and 69.91% into account and including the di-lepton modes of the Z boson (BR = 6.729% for e^+e^- and $\mu^+\mu^-$), the efficiencies for detecting a WW, WZ, ZZ pair originating from a partonic WW, WZ, ZZ final state are 35.4, 40.1 and 45.5%, respectively.

A significant part of the $VV\nu\nu$ final state is contributed by triple vector-boson production, where the third boson is a Z with invisible decay to neutrinos, cf. Fig. 3 (right). This might be considered as a separate background, and it is tempting to calculate this via a separate calculation of triple vector-boson production with Z decay. However, the process is probed in a kinematical region where the would-be Z boson is far off shell. The distribution in this region cannot be defined in a gauge-invariant way if we select only diagrams with a virtual Z boson. We have compared the results of [17,18], which were obtained for this selection of Feynman diagrams using 't Hooft–Feynman gauge for the gauge bosons, with an analogous WHIZARD calculation where all amplitudes are computed in unitarity gauge. As one may expect, the two results differ by a large factor in the signal region of high $\bar{\nu}\nu$ invariant masses, while coinciding on the Z mass peak. The momentum factors in the unitarity-gauge propagators produce a gauge-dependent excess which is cancelled against a matching piece if the full gauge-invariant set of diagrams is taken into account. In Tables 1 and 2, we quote the unitarity-gauge results for the three-boson subprocess for completeness, but we emphasize that after cuts, this number is unphysical and actually irrelevant for the signal sensitivity; as a background, it can be ignored for all practical purposes.

In other words, such a selection of Feynman graphs should not be attempted and a triple-boson background contribution cannot be defined. For the remainder of our study we only use results for the complete process which are gauge invariant by construction.

Besides gauge-invariance issues, we should note that the VVZ contribution to the processes of interest does not depend significantly on the coefficients of the operators in Eq. (19). This is easily understood if we remember that in the high-energy limit gauge and Goldstone bosons decouple. An intermediate off-shell Z or γ couples to a massless fermion current and therefore behaves as a gauge boson. A Goldstone-boson contribution is excited only via mixing, suppressed by $m_Z/\sqrt{s}$. Indeed we observe that in the low-mass region

for the neutrino system where the Z decay contributes, the dependence on the anomalous parameters is negligible. We can therefore cut on high VV invariant mass without losing sensitivity and thus concentrate on the genuine VBS topology. This property also removes any need for unitarizing the triple-production channel, since the SM contribution is guaranteed to respect perturbative unitarity.

6 Results for the minimal model

We now consider the minimal extrapolated EFT, properly unitarized, as a straightforward extension of the SM for VBS at high energy. We use the SM Lagrangian (18) and add the two dimension-eight operators (19) with their coefficients $F_{S,0}$ and $F_{S,1}$ as free parameters. The calculation is analogous to the LHC case [62]; for the numerical results, we use the model implementation in the WHIZARD event generator and the automatic calculation of unitarized tree-level amplitudes, distributions, and cross sections.

At low energy, the free parameters $F_{S,0}$ and $F_{S,1}$ are identified as expansion parameters in the EFT, within the range of validity of the latter.[3] For covering the whole kinematical range accessible at the LHC, we have to continue the amplitudes and cross sections into energy ranges where the EFT power-counting breaks down, interactions become strong, and the EFT result would violate unitarity. We therefore apply T-matrix unitarization to arrive at a unitary model. In effect, we obtain a smooth transition to high-energy asymptotics with saturation of unitarity in all partial waves. This is a two-parameter simplified model for a structureless strongly interacting continuum.

This expectation is confirmed by the numerical results which we display in Figs. 4, 5 and 6. In the plotted distributions, we choose exemplary values for the model parameters. As in the SM results listed above, all distributions are shown for unpolarized, structureless e^+e^- beams.

The result of this calculation can be expressed in terms of exclusion contours in a two-dimensional parameter space, centered on the SM as reference point. The exclusion contours are based on the hypothesis that no deviations from the SM are observed in an experiment. Given that our estimates follow from a simple cut-based analysis, we find it sufficient to calculate a small number of parameter points and suitably interpolate. In Fig. 7, we show the results for the sensitivity to $F_{S,0}$ and $F_{S,1}$. In addition to the exclusion contours that we obtain for the W^+W^- and ZZ final states, respectively, we indicate a 90 % exclusion limit that would be deduced from combining both channels. As it turns out, the ZZ channel is rather blind to one particular combination of parameters, resulting in the elongated blue shapes in the plots. The W^+W^- channel is more sensitive to both parameters and narrows down the shape in the combination of channels. In the combined result, the exclusion limits on both parameters are still correlated, as one would expect from the analogous results for the no-Higgs case [17,18].[4] Comparing the three selected collider energies, we conclude that increasing the energy from 1 to 3 TeV improves the sensitivity by roughly one order of magnitude, ultimately $\Delta F_{S,0/1} \sim 5\,\text{TeV}^{-4}$. These results may be compared to the run-I LHC limit on the same parameters, as obtained by ATLAS [7], $\Delta F_{S,0/1} \sim 500\,\text{TeV}^{-4}$ (cf. [48] for the conversion of exclusion limits).

In Fig. 8, we repeat the same analysis for an assumed beam polarization of 80 % (e^-), 0 % (e^+). The polarization effect enhances the signal more than the background and thus improves the sensitivity by another factor of 1.5. Finally, Fig. 9 displays the same 90 % exclusion contours with polarization for all three energy values in a common plot, for convenience of the reader.

We deliberately have included only the two channels W^+W^- and ZZ. Additional information can be gained by evaluating the other possible final states. However, these channels suffer from a larger fraction of γ-induced background and add independent information only if we relax the custodial-symmetry assumption, such that W and Z states are no longer related. For the current analysis, additional channels are of minor importance.

The sensitivity range for the anomalous coupling is of the order $1/\Lambda^4_{\text{eff}}$, where the effective scale Λ_{eff} is given by the W/Z pair energy where the differential distribution is maximal, cf. Fig. 5. This is the region where the anomalous couplings have the strongest impact – at low energies, their effect is naturally suppressed, while at high energies, unitarity becomes saturated and the sensitivity disappears again. Clearly, the measurement is limited by statistics.

For the purpose of this study, we rely only on the total cross section within a fiducial phase space which is isolated by the cut strategy as described above. Further details can be deduced from the vector-boson pair invariant mass distribution, as displayed in the figures. The availability of this important observable, in form of the total hadronic energy and momentum, is a great advantage of the clean lepton-collider environment, as compared to the situation at a hadron collider.

[3] In the ATLAS analysis of VBS at the LHC [6], the notation (α_4, α_5) was adopted instead, borrowed from the no-Higgs EFT [47], although the theory model included the light Higgs and unitarization, i.e., worked with the extrapolated EFT model of the present paper. For the relation of coefficients, cf. [44].

[4] The correlation could in principle be reduced by a measurement of the W^-W^- channel [63], but this requires an e^-e^- mode which is not foreseen for the CLIC project.

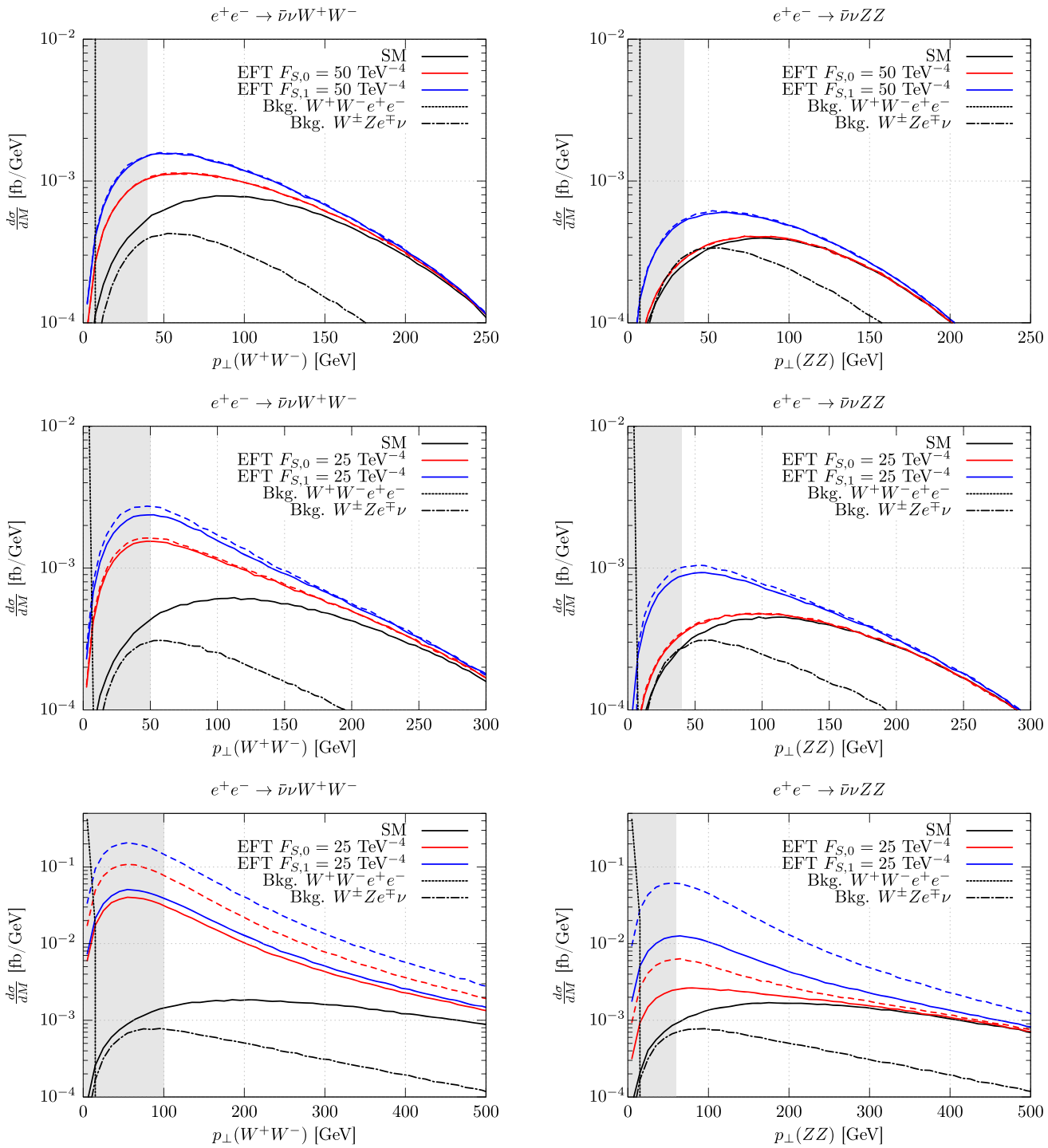

Fig. 4 Differential cross sections depending on the transverse momentum of the W (*left plots*) and the Z boson pair (*right plots*) at center-of-mass energies of 1 TeV (*upper plots*), 1.4 TeV (*middle plots*) and 3 TeV (*lower plots*). The *solid lines* show the signal process $\bar{\nu}\nu W^+W^-(ZZ)$ with SM values $F_{S,0} = F_{S,1} = 0$. The *red/blue lines* indicate the signal process with non-SM value $F_{S,0,1} = 25/50$ TeV^{-4} (*dashed lines* naive EFT results, *solid lines* unitarized results). In addition, the two SM background processes $W^+W^-e^+e^-$ and $W^\pm Ze^\mp\nu$ (with 13.6% misidentification probability) are also plotted. The *shaded area* is removed by the cut on the $W(Z)$ boson system. All other cuts have been applied as described. No detection efficiencies are included

A complete experimental analysis, which is beyond the scope of the present paper, should take the simulation results and apply a proper fitting procedure that takes into account all available information. Such an analysis of VBS data would exploit a complete set of observables. In particular, it will be advantageous to resolve the decay prod-

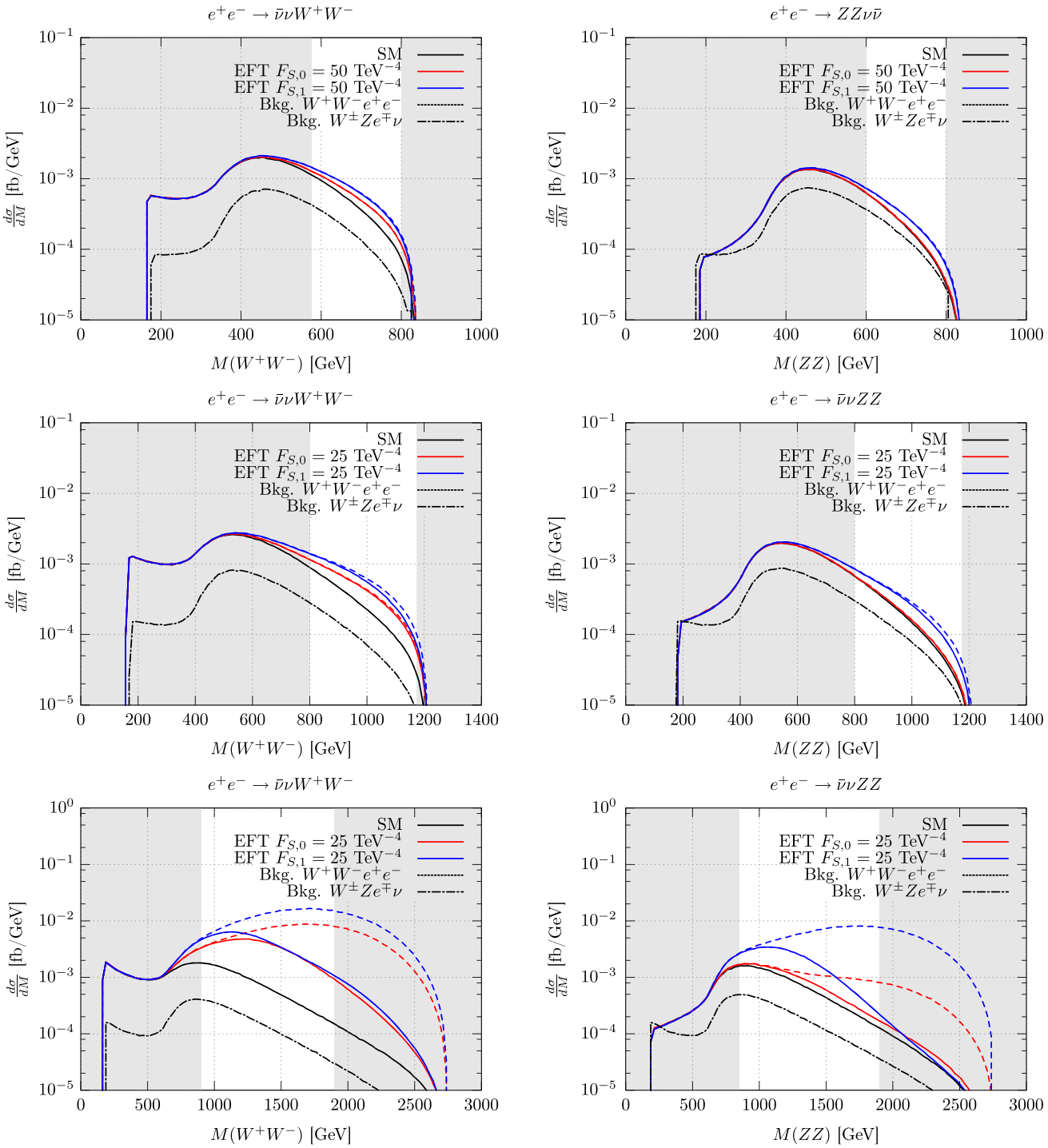

Fig. 5 Differential cross sections depending on the invariant mass of the W (*left plots*) and the Z boson pair (*right plots*) at center-of-mass energies of 1 TeV (*upper plots*), 1.4 TeV (*middle plots*) and 3 TeV (*lower plots*). The *solid lines* show the signal process $\bar{\nu}\nu W^+W^-(ZZ)$ with SM values $F_{S,0} = F_{S,1} = 0$. The *red/blue lines* indicate the signal process with non-SM value $F_{S,0,1} = 25/50$ TeV^{-4} (*dashed lines* naive EFT results, *solid lines* unitarized results). In addition, the two SM background processes $W^+W^-e^+e^-$ and $W^\pm Ze^\mp\nu$ (with 13.6% misidentification probability) are also plotted. The *shaded area* is removed by the cut on the $W(Z)$ boson system. All other cuts have been applied as described. No detection efficiencies are included

ucts of the vector bosons into individual jets – quarks in the language of the partonic elementary process – and take into account their angular and energy distributions. For illustration of the added value, we have generated WHIZARD event samples for the complete exclusive process $e^+e^- \to \bar{\nu}\nu + 4j$ with all possible Feynman graphs included,

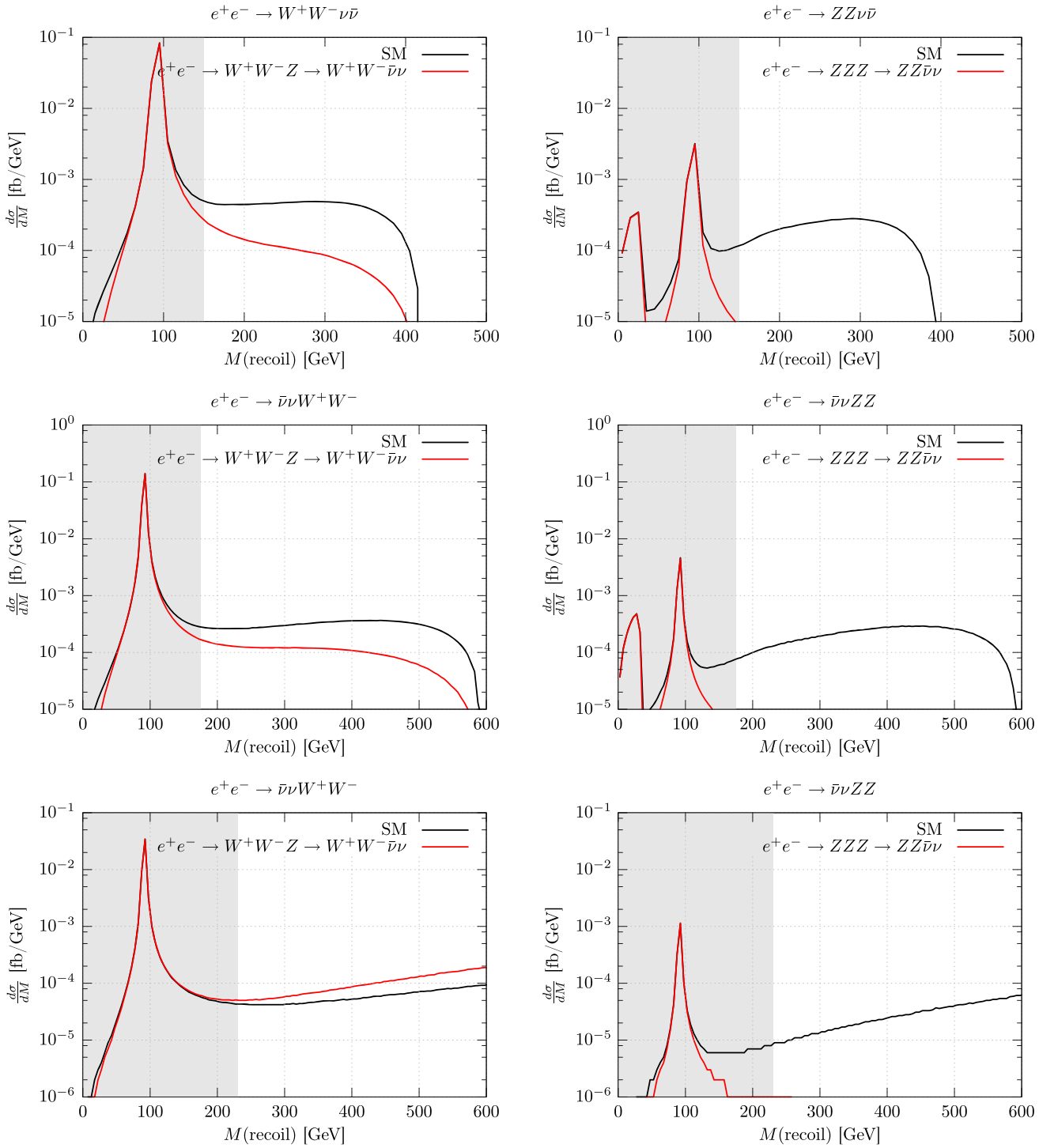

Fig. 6 Differential cross sections depending on the recoil mass of the W (*left plots*) and the Z boson pair (*right plots*) at center-of-mass energies of 1 TeV (*upper plots*), 1.4 TeV (*middle plots*) and 3 TeV (*lower plots*). The *solid lines* show the signal process $\bar{\nu}\nu W^+W^-(ZZ)$. The *red lines* show the background process $e^+e^- \to W^+W^-(ZZ)Z \to W^+W^-(ZZ)\nu\bar{\nu}$, where the two neutrinos are generated through a decaying Z boson. The *shaded area* is removed by the cut on the neutrino system. All other cuts have been applied as described above. No detection efficiencies are included

summed over neutrino and quark flavors, for the SM and for some nonzero values of the EFT operator coefficient $F_{S,0}$, Fig. 10.

In this figure, we show the distribution in the polar angle θ^* between the final-state jets in the rest frame of the parent (off-shell) vector boson. This cut is applied at Monte Carlo truth

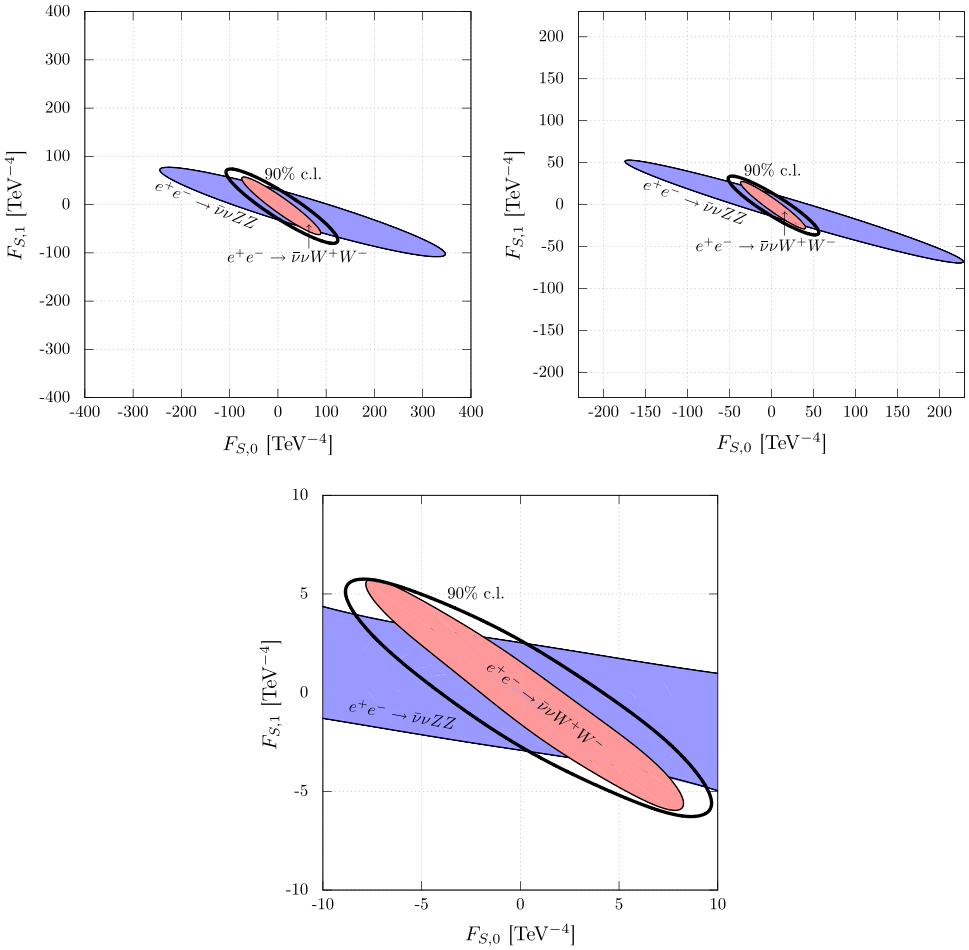

Fig. 7 $\pm 1\sigma$ exclusion contours in the $F_{S,0}/F_{S,1}$ plane for the two signal processes $e^+e^- \to \bar{\nu}\nu W^+W^-$ and $e^+e^- \to \bar{\nu}\nu ZZ$ including all background processes based on the assumption $F_{S,0} = F_{S,1} = 0$. The $e^-(e^+)$ beam is unpolarized at energies of 1.0 TeV (*upper left plot*), 1.4 TeV (*upper right plot*) and 3 TeV (*lower plot*). The corresponding integrated luminosities are 5, 1.5 and 2 ab^{-1}, respectively. All cuts have been applied and detection efficiencies are included. The *thick line* indicates the 90% exclusion sensitivities obtained by the combination of the two signal channels. All *cross sections* are unitarized

level to both jet pairs including all combinatorics. Expanding on this result, to enhance the vector-boson scattering signal further above the background, the following cut on the angle θ^* could be used (as before: first number applies for 3 TeV and the number in brackets for 1.4 TeV):

$$0.2(0.4) < |\cos(\theta^*)| < 0.75 \tag{22}$$

A more sophisticated analysis would exploit the complete information from this distribution and add in any further observable that provides discriminating power.

7 Results for resonance models

Besides the extrapolated EFT of the previous section, we now consider a second set of models for VBS at high energy. Starting again from the Lagrangian (18), we add a field with high mass, definite $SU(2)_L \times SU(2)_R$ quantum numbers and with a minimal coupling to a Higgs–Goldstone current in the Lagrangian, as a possible resonance. For concreteness, we adopt resonance quantum numbers and parameters that we did study for the LHC in Ref. [62], and specifically select three models, namely an isoscalar–scalar σ, an isotensor–scalar ϕ, and an isoscalar–tensor f. For each model, we introduce the resonance mass and the coupling to the Higgs current as two independent new parameters. Ignoring further decay channels, the coupling and mass also determine the width of the resonance.

Such simplified models collect features of a wide variety of complete models. They range from Higgs-singlet models and other extended Higgs sectors to strongly interacting scenarios where, due to Higgs compositeness or some other underlying BSM mechanism, resonances with varying spin or isospin should appear that are coupled to the physical Higgs doublet but not necessarily to the fermionic sector. In general, any new resonance will also have gauge interactions and, because we are typically in a strong-interaction regime, anomalous moments that effectively provide higher-dimensional couplings to the gauge degrees of freedom, i.e., transversal vector bosons. The isospin representation does not uniquely determine the gauge couplings. For instance, an isospin-two resonance multiplet can originate in the decomposition of $(2,0)$, $(1,1)$, $(0,2)$, or higher representations under $SU(2)_L \times SU(2)_R$. For the $(0,2)$ quantum-number assignment in particular, there is only a coupling to hypercharge. The resulting extra interactions give rise to new processes with multiple vector bosons in the final state at high

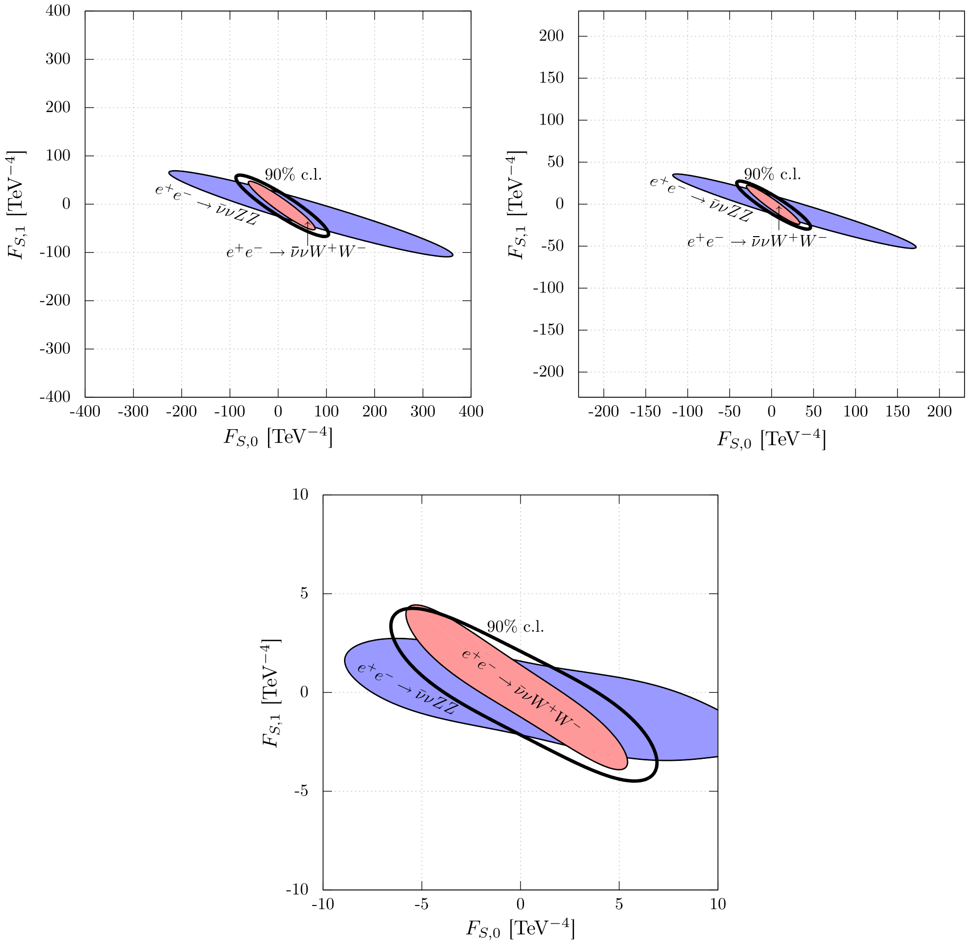

Fig. 8 $\pm 1\sigma$ exclusion contours in the $F_{S,0}/F_{S,1}$ plane for the two signal processes $e^+e^- \to \bar{\nu}\nu W^+W^-$ and $e^+e^- \to \bar{\nu}\nu ZZ$ including all background processes based on the assumption $F_{S,0} = F_{S,1} = 0$. The $e^-(e^+)$ beam is polarized at a degree of 80%(0%) at energies of 1.0 TeV (*upper left plot*), 1.4 TeV (*upper right plot*) and 3 TeV (*lower plot*). The corresponding integrated luminosities are 5 ab^{-1}, 1.5 ab^{-1} and 2 ab^{-1}, respectively. All cuts have been applied and detection efficiencies are included. The *thick line* indicates the 90% exclusion sensitivities obtained by the combination of the two signal channels. All *cross sections* are unitarized

energy. In addition to the operators above there can be couplings to pure gauge currents with arbitrary coefficients. All couplings to the gauge degrees of freedom are, however, parametrically suppressed by gauge-coupling factors. In accordance with the Goldstone-boson limit where the gauge couplings are formally set to zero, we choose to keep our simplified models as simple as possible and do not take such effects into account in the present work.

With these simplifications, the model Lagrangians for the three fields σ, f, ϕ are

$$\mathcal{L}_\sigma = \frac{1}{2}\partial_\mu\sigma\partial^\mu\sigma - \frac{1}{2}m_\sigma^2\sigma^2 + \sigma J_\sigma \tag{23a}$$

$$\mathcal{L}_\phi = \frac{1}{2}\sum_{i=s,v,t}\mathrm{tr}\left[\partial_\mu\Phi_i\partial^\mu\Phi_i - m_\Phi^2\Phi_i^2\right] + \mathrm{tr}\left[\left(\Phi_t + \frac{1}{2}\Phi_v - \frac{2}{5}\Phi_s\right)J_\phi\right], \tag{23b}$$

$$\mathcal{L}_f = \frac{1}{2}\partial_\alpha f_{\mu\nu}\partial^\alpha f^{\mu\nu} - \frac{1}{2}m^2 f_{\mu\nu}f^{\mu\nu} - \partial^\alpha f_{\alpha\mu}\partial_\beta f^{\beta\mu} - f^\alpha_\alpha\partial^\mu\partial^\nu f_{\mu\nu} - \frac{1}{2}\partial_\alpha f^\mu_\mu\partial^\alpha f^\nu_\nu + \frac{1}{2}m^2 f^\mu_\mu f^\nu_\nu + f_{\mu\nu}J_f^{\mu\nu}, \tag{23c}$$

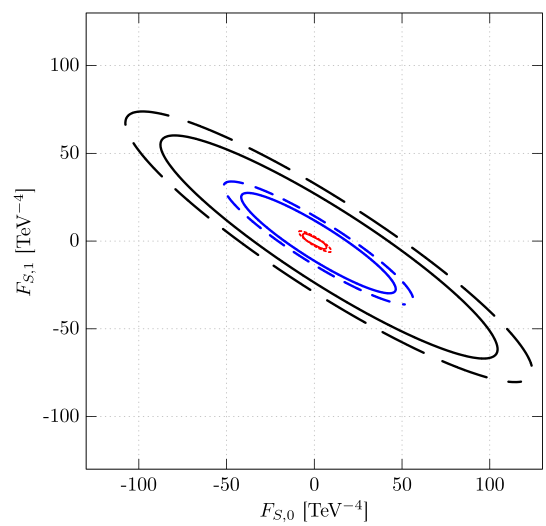

Fig. 9 90 % exclusion sensitivities for polarized (*solid*) and unpolarized (*dashed*) particle beams at energies of $\sqrt{s} = 1$ (*black/outermost*), 1.4(*blue/middle*), 3 TeV(*red/innermost*) combined, assuming integrated luminosities of 5, 1.5 and 2 ab^{-1}, respectively

where J_σ, J_ϕ, J_f are the currents which couple to the new fields, respectively. We note that the isotensor–scalar ϕ, defined by its $SU(2)_R \times SU(2)_L$ quantum numbers $\mathbf{1} \times \mathbf{1}$,

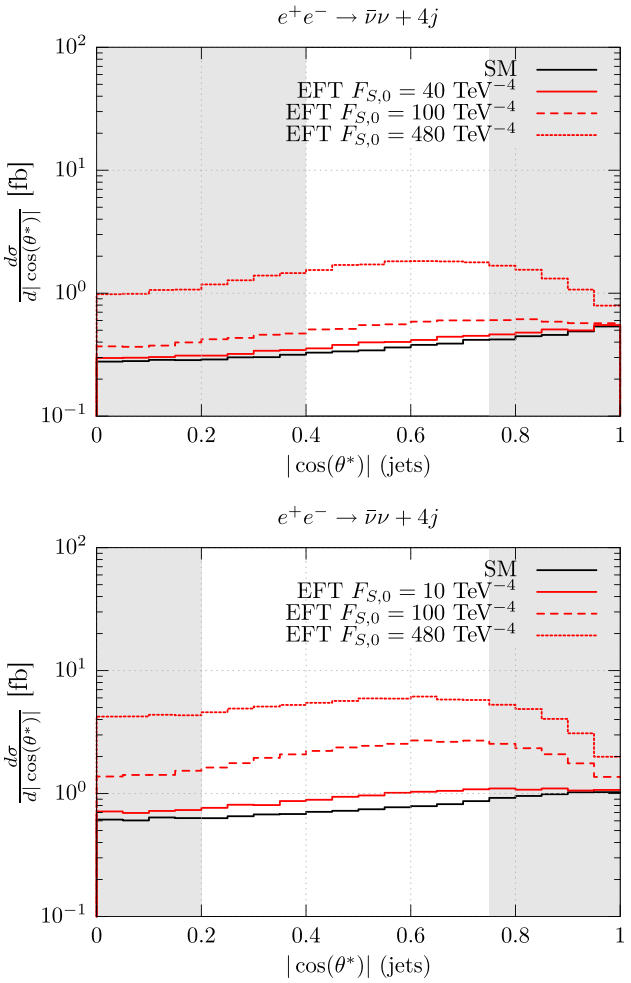

Fig. 10 Differential cross sections of the process $e^+e^-\bar{\nu} \to \nu + 4j$ at center-of-mass energies of 1.4 TeV (*top plot*) and 3 TeV (*bottom plot*) depending on the jet pairs $|cos(\theta^*)|$ at different values of $F_{S,0}$. All cuts have been applied as described above. No detection efficiencies are included and all cross sections are unitarized

decomposes after electroweak symmetry breaking into an isotensor Φ_t, an isovector Φ_v and isoscalar Φ_s transforming under custodial $SU(2)$.

The currents that interact with the resonances are given by the Higgs doublet and its derivative,

$$J_\sigma = F_\sigma \operatorname{tr}\left[\left(\mathbf{D}_\mu \mathbf{H}\right)^\dagger \mathbf{D}^\mu \mathbf{H}\right], \tag{24a}$$

$$J_\phi = F_\phi \left(\left(\mathbf{D}_\mu \mathbf{H}\right)^\dagger \otimes \mathbf{D}^\mu \mathbf{H} + \frac{1}{8}\operatorname{tr}\left[\left(\mathbf{D}_\mu \mathbf{H}\right)^\dagger \mathbf{D}^\mu \mathbf{H}\right]\right) \tau^a \otimes \tau^a, \tag{24b}$$

$$J_f^{\mu\nu} = F_f \left(\operatorname{tr}\left[\left(\mathbf{D}^\mu \mathbf{H}\right)^\dagger \mathbf{D}^\nu \mathbf{H}\right] - \frac{c_f}{4} g^{\mu\nu} \operatorname{tr}\left[\left(\mathbf{D}_\rho \mathbf{H}\right)^\dagger \mathbf{D}^\rho \mathbf{H}\right]\right). \tag{24c}$$

For further details, cf. [62].

At low energy, each of the three resonance models reduces to a one-parameter effective theory, since a single combination of mass and coupling parameters enters into effective values of $F_{S,0}$ and $F_{S,1}$. These models therefore provide high-energy extensions of the generic low-energy EFT, as alternatives to the straightforward extrapolation of the preceding section. The resonance models exhibit more structure than the simple extrapolation. All models require unitarization, which we again implement using the T-matrix framework, since the interaction operators introduce terms that rise with energy.

If the effect of the new states is to be sizable and thus observable, the interactions should be rather strong, so generically we do not expect a renormalizable model with tree-level unitary asymptotics. Nevertheless, weakly interacting models such as a UV-complete Higgs-singlet model are included in this model space. For a renormalizable model, any terms that apparently rise with energy would cancel against higher-order contributions. From a phenomenological perspective, renormalizable models are exceptional points in a larger parameter space that we cover by the above definitions.

In Fig. 11, we display the vector-boson pair invariant mass distribution for the SM with an additional isoscalar scalar resonance σ, equivalent to an extra Higgs-like singlet boson. The plots show both the W^+W^- final state (left column) and the ZZ final state (right column). We have chosen a moderately high mass of $M_\sigma = 800$ GeV and a rather small width of $\Gamma_\sigma = 80$ GeV (blue curve). The distribution, which for the full process translates into the invariant mass of the hadronic (four-jet) system, shows an unambiguous peak at the resonance mass that is distinguishable in shape from the SM background (black), given sufficient luminosity. The peak is more pronounced for 3 TeV collider energy, but also clearly visible for 1.4 TeV. It is evident that, for this choice of parameters, the formally correct EFT expansion (red curve) does not aproximate the actual model behavior at all. Unitarization does not play a significant role except for the naively extrapolated EFT (dashed red) which overshoots the unitarized curves (solid), and thus the unitarity bounds, by a substantial amount.

The plots in Fig. 12 depict a somewhat lighter isoscalar–scalar resonance ($M_\sigma = 650$ GeV) with a larger width ($\Gamma_\sigma = 260$ GeV). In this case, the resonance shape follows the shape of the extrapolated EFT but leads to at significantly larger peak cross section. Since the equivalent EFT parameter, matching to the slope of the resonance curve below threshold, is twice as large as in the previous set of plots, the unphysical behavior is evident that we would get without unitarization (dashed curves). This applies not just to the EFT approximation (red), but also to the resonance curves (blue).

In Fig. 13, we consider an isoscalar tensor resonance with $M_f = 1$ TeV and $\Gamma_f = 100$ GeV, which produces a rather

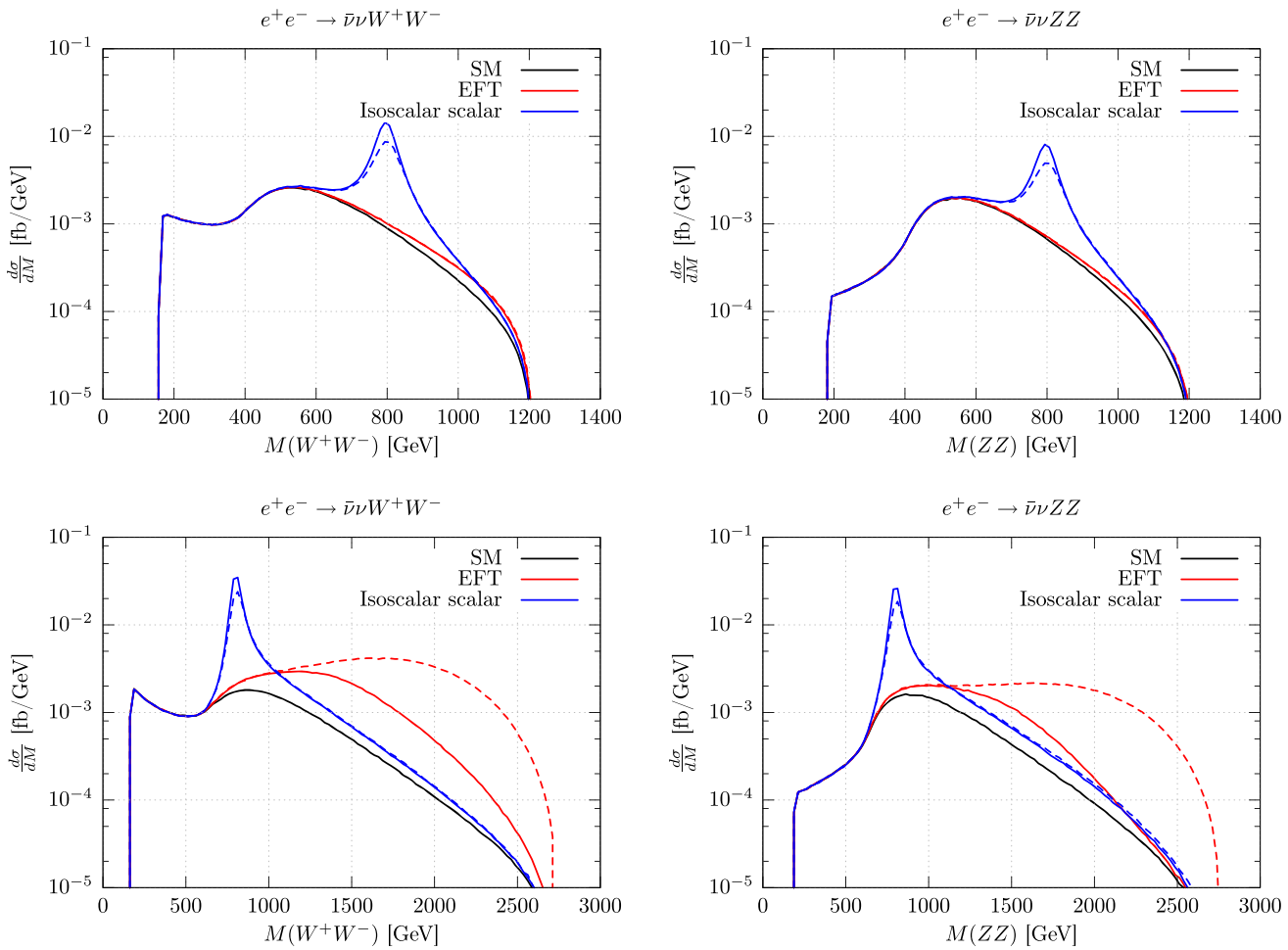

Fig. 11 Differential cross sections including a weakly coupled isoscalar scalar resonance ($m_\sigma = 800$ GeV, $F_\sigma = 4.0$ TeV^{-1}, $\Gamma_\sigma = 80$ GeV) depending on the invariant mass of the vector-boson pair at center-of-mass energies of $\sqrt{s} = 1.4$ TeV (*upper plots*) and $\sqrt{s} = 3$ TeV (*lower plots*). *Plots on the left* show the process $e^+e^- \to \bar{\nu}\nu W^+W^-$, *plots on the right* $e^+e^- \to \bar{\nu}\nu ZZ$. *Blue line* isoscalar scalar resonance, *red line* matched EFT results ($F_{S,0} = 0$, $F_{S,1} = 12.3$ TeV^{-4}). *Solid line* unitarized results, *dashed line* naive results

narrow peak in all distributions. With a collider energy of 3 TeV, we observe the necessity for unitarization beyond the mass peak (in the WW final state), caused by the dimensionality of the effective tensor–scalar interaction. As well as in all other cases, if we had a UV-complete model at hand, we would expect any variation of the resonance-model prediction (blue) in this range: further resonances, a featureless continuum, or suppression that accommodates the emergence of further inelastic channels. However, neither of these scenarios could produce a unitarity-violating result like the naive blue-dashed line, so the unitarized model prediction serves as a conservative estimate of the asymptotic shape.

The final parameter set in Fig. 14, an isotensor–scalar multiplet ϕ, illustrates a possible strongly interacting multi-Higgs scenario. The broad resonance, actually a combination of resonance exchange in all isospin channels, is indistinguishable from an arbitrary continuum. It is remarkable that the EFT approximation follows the shape of the resonance model in the WW final state but fails completely for the ZZ final state. As before, the naive extrapolations (dashed) overshoot the unitarized models (solid) by a large amount.

8 Conclusions

We have performed a new study of the capability of a high-energy lepton collider (such as CLIC or an upgraded ILC) to measure quasi-elastic vector-boson scattering, as a dedicated probe of the Higgs sector. For realistic luminosity-energy combinations, we cannot restrict the investigation to a pure effective field theory (EFT), but have to take into account strong interactions or resonant behavior.

Specifically, we have considered a minimal unitary extrapolation of the EFT Lagrangian and related this to alterna-

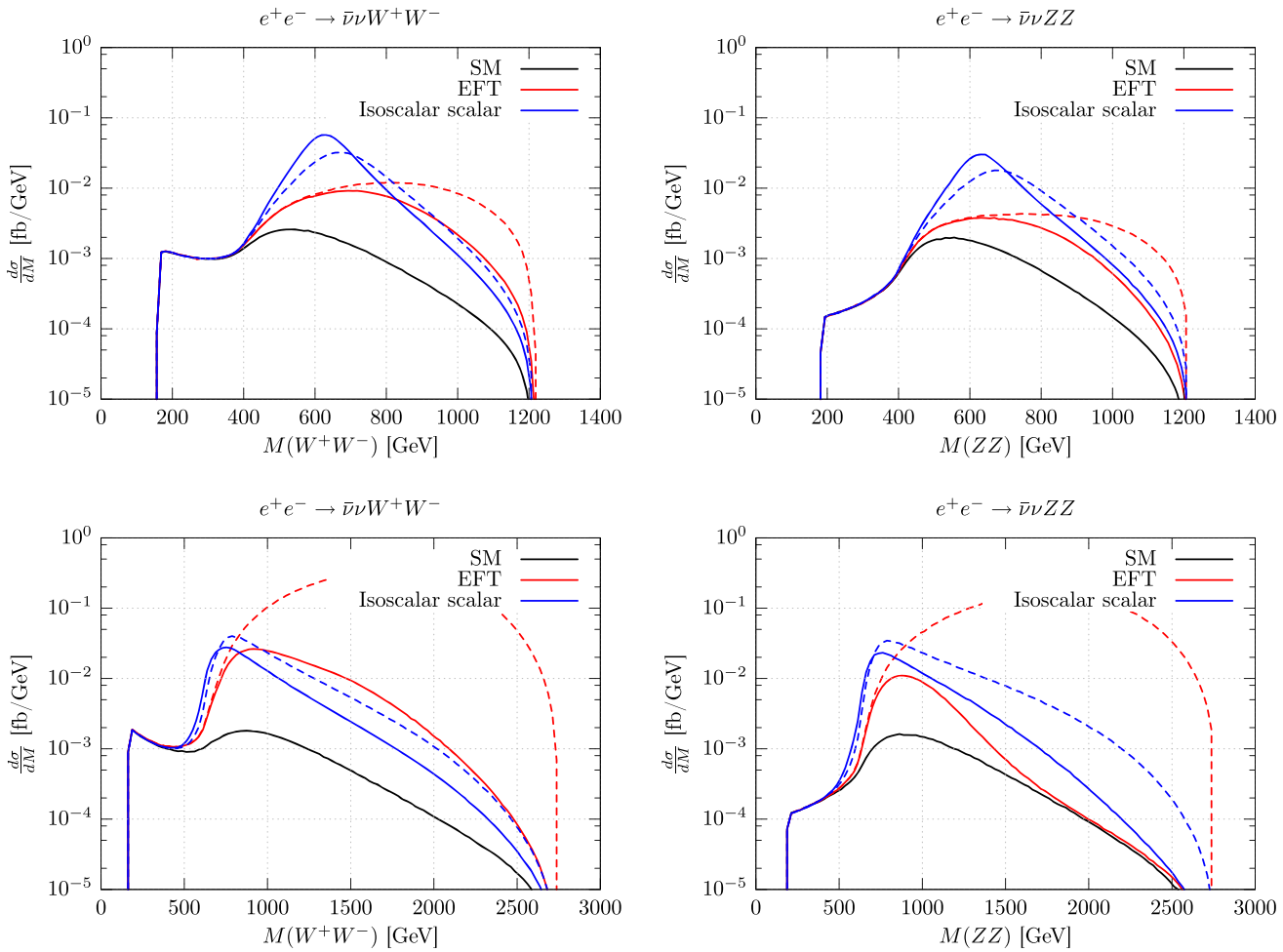

Fig. 12 Differential cross sections including a low lying isoscalar scalar resonance ($m_\sigma = 650$ GeV, $F_\sigma = 9.8$ TeV^{-1}, $\Gamma_\sigma = 260$ GeV) depending on the invariant mass of the vector-boson pair at center-of-mass energies of $\sqrt{s} = 1.4$ TeV (*upper plots*) and $\sqrt{s} = 3$ TeV (*lower plots*). *Plots on the left* show the process $e^+e^- \to \bar{\nu}\nu W^+W^-$, *plots on the right* $e^+e^- \to \bar{\nu}\nu ZZ$. *Blue line* isoscalar scalar resonance, *red line* matched EFT results ($F_{S,0} = 0$, $F_{S,1} = 112.6$ TeV^{-4}). *Solid line* unitarized results, *dashed line* naive results.

tive models where the anomalous effects develop into resonances within the kinematical range. This set of simplified models covers a range of possibly asymptotic behavior. All scenarios reduce to the standard model with leading higher-dimensional corrections at the low-energy threshold for vector-boson scattering processes. The T-matrix unitarization framework lets us implement the unitarity condition for all models by a universal algorithm and simultaneously allows us to embed them in a full off-shell calculation and Monte-Carlo simulation. For the purpose of working with fully exclusive event samples, all models have been implemented in the public version of the WHIZARD Monte-Carlo event generator.

The results yield an overview over the experimental reach of the CLIC and ILC colliders in the various scenarios. Using optimized cuts for longitudinal vector-boson scattering, we generically obtain a sensitivity on the unitarized-EFT parameters $F_{S,0}$ and $F_{S,1}$ of $O(1/\Lambda^4)$, where Λ indicates the location of the maximum of the unitarized cross section, in terms of the vector-boson pair invariant mass as the relevant energy scale. In contrast to an unphysical, naively extrapolated EFT, the main sensitivity in the unitary model does not originate from the highest energies, but from the energy range around Λ where the cross section is maximal. Due to the universal damping imposed by unitarity, the asymptotic region is suppressed in the results, such that only a minor fraction of the actual event rates can be influenced by the high-energy behavior of the chosen model.

The minimal model thus provides a smooth interpolation between the two-parameter low-energy EFT and a saturated continuum at high energy. As our numerical results indicate, the free parameters which we identify with EFT operator coefficients effectively describe the location and shape of the cross-section peak, which falls in the transition region. Given

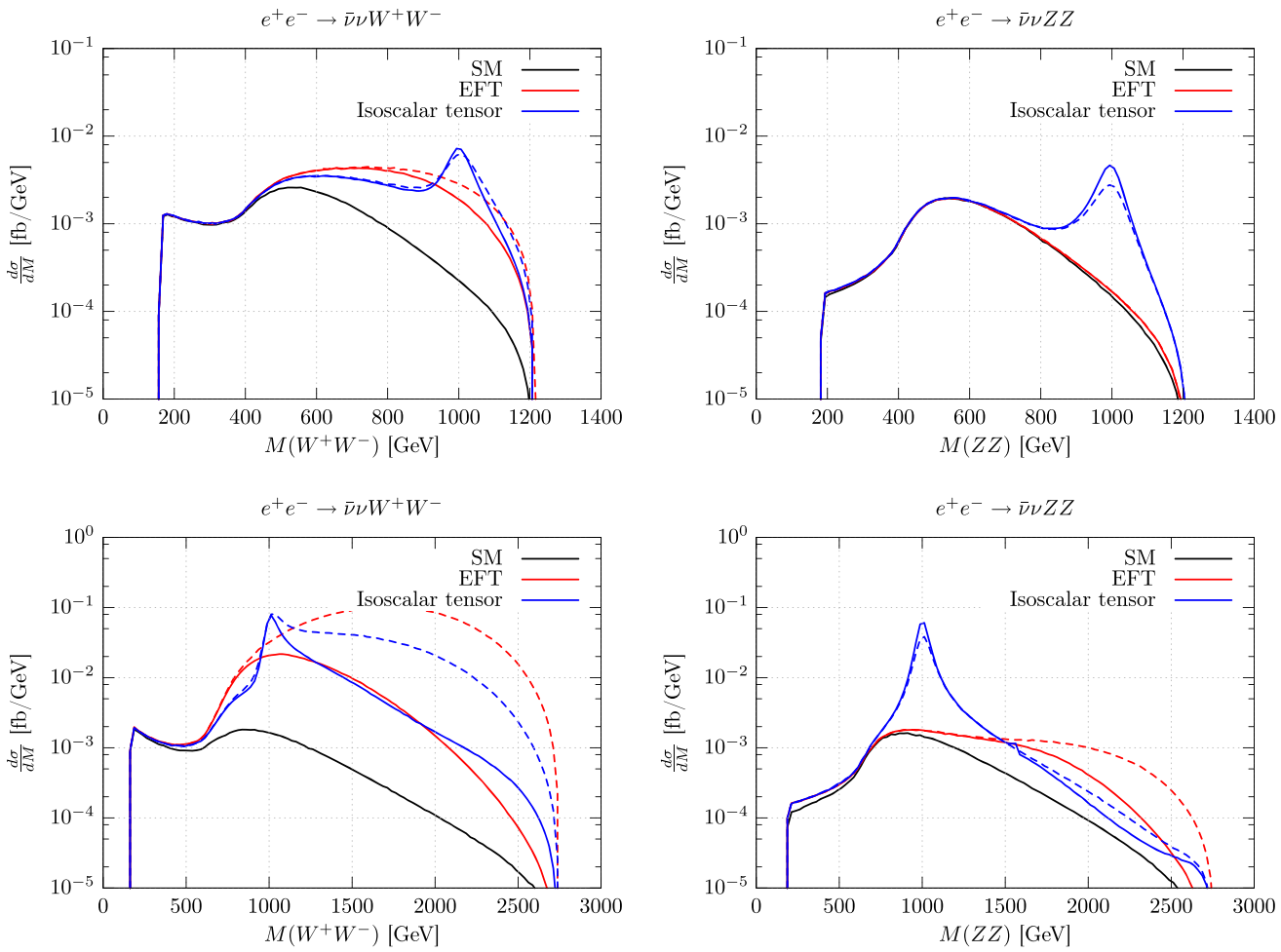

Fig. 13 Differential cross sections including an isoscalar tensor resonance ($m_f = 1000$ GeV, $F_f = 17.4$ TeV^{-1}, $\Gamma_f = 100$ GeV) depending on the invariant mass of the vector-boson pair at center-of-mass energies of $\sqrt{s} = 1.4$ TeV (*upper plots*) and $\sqrt{s} = 3$ TeV (*lower plots*). *Plots on the left* show the process $e^+e^- \to \bar{\nu}\nu W^+W^-$, *plots on the right* $e^+e^- \to \bar{\nu}\nu ZZ$. *Blue line* isoscalar tensor resonance, *red line* matched EFT results ($F_{S,0} = 150.8$ TeV^{-4}, $F_{S,1} = -50.3$ TeV^{-4}). *Solid line* unitarized results, *dashed line* naive results

this property, one may ask about the possible influence of extra parameters that at low energy reduce to operator coefficients of even higher dimension. A complete theory will provide an infinite series of higher-dimensional operators, all of them contributing in the transition region. The resulting peak shape will depend on all parameters. Such detail becomes phenomenologically relevant if significant additional structure is generated in the measured distributions.

We account for the possibility of additional structure by studying resonance models as an alternative. When the peak shape becomes experimentally resolvable with sufficient precision, a refinement of the minimal structureless model becomes phenomenologically relevant. However, unless the new-physics scale is rather low, it requires substantial luminosity to achieve such a level of precision at the CLIC collider. Therefore, refining the model by introducing further parameters does not appear to be justified at the current stage. Any calculation that matches a specific UV model to the phenomenological parameterization, has to take this type of ambiguity into account.

Regarding resonance models, we have restricted ourselves to a few exemplary parameter points in this exploratory study, which should be representative of the phenomenology that can be expected. For precise and systematic parameter determinations, the specific models should be subject to an experimental fitting procedure and analysis which takes into account complete event information and weighs the distributions according to their sensitivity to the specific model in question.

The expected sensitivity of the CLIC collider with 3 TeV, as expressed for the parameters of the extrapolated EFT as the simplest model, improves over the current LHC limits by two orders of magnitude. Clearly, the CLIC expectation has to be compared to the ultimate precision achievable by

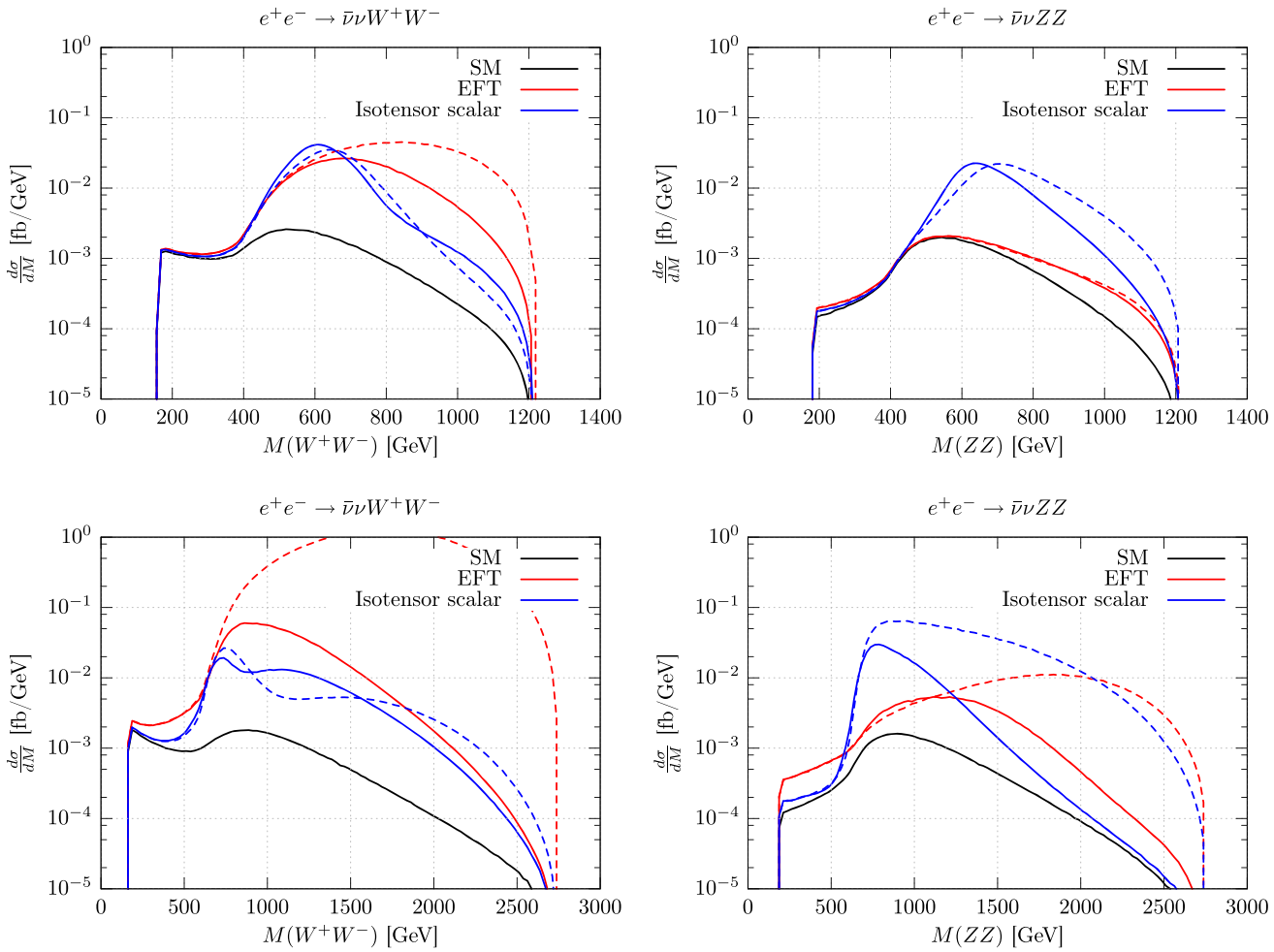

Fig. 14 Differential cross sections including a low lying isotensor scalar resonance ($m_\phi = 650$ GeV, $F_\phi = 19.5$ TeV^{-1}, $\Gamma_\phi = 260$ GeV) depending on the invariant mass of the vector-boson pair at center-of-mass energies of $\sqrt{s} = 1.4$ TeV (*upper plots*) and $\sqrt{s} = 3$ TeV (*lower plots*). *Plots on the left* show the process $e^+e^- \to \bar{\nu}\nu W^+W^-$, *plots on the right* $e^+e^- \to \bar{\nu}\nu ZZ$. *Blue line* isotensor scalar resonance, *red line* matched EFT results ($F_{S,0} = 450.5$ TeV^{-4}, $F_{S,1} = -112.6$ TeV^{-4}). *Solid line* unitarized results, *dashed line* naive results

the LHC experiments. A detailed comparison of sensitivities would require applying the available analysis techniques to a full-simulation prediction for either collider, which is beyond the scope of the present paper. However, the e^+e^- environment allows for the detection of well-defined final states, hadronic decays, and a direct measurement of the most relevant distribution – the vector-boson pair invariant mass – and thus remains the preferred setup for a comprehensive study of VBS in the TeV energy range.

Acknowledgements We would like to thank Lucie Linssen, Philipp Roloff, and Marcel Vos for enlightening discussions on the CLIC project. MS acknowledges the support of BMBF Verbundforschung (HEP Theory).

Appendix A: Dimension-eight operators that affect VBS

The following list of dimension-eight operators includes all leading interactions that modify the SM form of VBS interactions. In the current paper, we restrict the investigation to the first set of operators which describes genuine Goldstone–Higgs self-interactions, which for completeness we repeat here from Eq. (19):

$$\mathcal{L}_{S,0} = F_{S,0}\ \mathrm{tr}\left[\left(\mathbf{D}_\mu \mathbf{H}\right)^\dagger \mathbf{D}_\nu \mathbf{H}\right] \mathrm{tr}\left[\left(\mathbf{D}^\mu \mathbf{H}\right)^\dagger \mathbf{D}^\nu \mathbf{H}\right], \quad \text{(A.1a)}$$

$$\mathcal{L}_{S,1} = F_{S,1}\ \mathrm{tr}\left[\left(\mathbf{D}_\mu \mathbf{H}\right)^\dagger \mathbf{D}^\mu \mathbf{H}\right] \mathrm{tr}\left[\left(\mathbf{D}_\nu \mathbf{H}\right)^\dagger \mathbf{D}^\nu \mathbf{H}\right]. \quad \text{(A.1b)}$$

Exchanging two covariant derivatives with field strength tensors, further possibilities arise to construct linearly independent operators

$$\mathcal{L}_{M,0} = -g^2 F_{M,0} \operatorname{tr}\left[\left(\mathbf{D}_\mu \mathbf{H}\right)^\dagger \left(\mathbf{D}^\mu \mathbf{H}\right)\right] \operatorname{tr}\left[\mathbf{W}_{\nu\rho}\mathbf{W}^{\nu\rho}\right], \tag{A.2a}$$

$$\mathcal{L}_{M,1} = -g^2 F_{M,1} \operatorname{tr}\left[\left(\mathbf{D}_\mu \mathbf{H}\right)^\dagger \left(\mathbf{D}^\rho \mathbf{H}\right)\right] \operatorname{tr}\left[\mathbf{W}_{\nu\rho}\mathbf{W}^{\nu\mu}\right], \tag{A.2b}$$

$$\mathcal{L}_{M,2} = -g'^2 F_{M,2} \operatorname{tr}\left[\left(\mathbf{D}_\mu \mathbf{H}\right)^\dagger \left(\mathbf{D}^\mu \mathbf{H}\right)\right] \operatorname{tr}\left[\mathbf{B}_{\nu\rho}\mathbf{B}^{\nu\rho}\right], \tag{A.2c}$$

$$\mathcal{L}_{M,3} = -g'^2 F_{M,3} \operatorname{tr}\left[\left(\mathbf{D}_\mu \mathbf{H}\right)^\dagger \left(\mathbf{D}^\rho \mathbf{H}\right)\right] \operatorname{tr}\left[\mathbf{B}_{\nu\rho}\mathbf{B}^{\nu\mu}\right], \tag{A.2d}$$

$$\mathcal{L}_{M,4} = -gg' F_{M,4} \operatorname{tr}\left[\left(\mathbf{D}_\mu \mathbf{H}\right)^\dagger \mathbf{W}_{\nu\rho} \left(\mathbf{D}^\mu \mathbf{H}\right) \mathbf{B}^{\nu\rho}\right], \tag{A.2e}$$

$$\mathcal{L}_{M,5} = -gg' F_{M,5} \operatorname{tr}\left[\left(\mathbf{D}_\mu \mathbf{H}\right)^\dagger \mathbf{W}_{\nu\rho} \left(\mathbf{D}^\rho \mathbf{H}\right) \mathbf{B}^{\nu\mu}\right], \tag{A.2f}$$

$$\mathcal{L}_{M,7} = -g^2 F_{M,7} \operatorname{tr}\left[\left(\mathbf{D}_\mu \mathbf{H}\right)^\dagger \mathbf{W}_{\nu\rho}\mathbf{W}^{\nu\mu} \left(\mathbf{D}^\rho \mathbf{H}\right)\right]. \tag{A.2g}$$

Here, we kept the numbering analog to the linear Higgs doublet representation in [44] for future comparisons, where some linear dependent operators of [42] are already omitted.

Operators affecting only the gauge bosons consist of four electroweak field strength tensors

$$\mathcal{L}_{T,0} = g^4 F_{T,0} \operatorname{tr}\left[\mathbf{W}_{\mu\nu}\mathbf{W}^{\mu\nu}\right] \operatorname{tr}\left[\mathbf{W}_{\alpha\beta}\mathbf{W}^{\alpha\beta}\right], \tag{A.3a}$$

$$\mathcal{L}_{T,1} = g^4 F_{T,1} \operatorname{tr}\left[\mathbf{W}_{\alpha\nu}\mathbf{W}^{\mu\beta}\right] \operatorname{tr}\left[\mathbf{W}_{\mu\beta}\mathbf{W}^{\alpha\nu}\right], \tag{A.3b}$$

$$\mathcal{L}_{T,2} = g^4 F_{T,2} \operatorname{tr}\left[\mathbf{W}_{\alpha\mu}\mathbf{W}^{\mu\beta}\right] \operatorname{tr}\left[\mathbf{W}_{\beta\nu}\mathbf{W}^{\nu\alpha}\right], \tag{A.3c}$$

$$\mathcal{L}_{T,5} = g^2 g'^2 F_{T,5} \operatorname{tr}\left[\mathbf{W}_{\mu\nu}\mathbf{W}^{\mu\nu}\right] \operatorname{tr}\left[\mathbf{B}_{\alpha\beta}\mathbf{B}^{\alpha\beta}\right], \tag{A.3d}$$

$$\mathcal{L}_{T,6} = g^2 g'^2 F_{T,6} \operatorname{tr}\left[\mathbf{W}_{\alpha\nu}\mathbf{W}^{\mu\beta}\right] \operatorname{tr}\left[\mathbf{B}_{\mu\beta}\mathbf{B}^{\alpha\nu}\right], \tag{A.3e}$$

$$\mathcal{L}_{T,7} = g^2 g'^2 F_{T,7} \operatorname{tr}\left[\mathbf{W}_{\alpha\mu}\mathbf{W}^{\mu\beta}\right] \operatorname{tr}\left[\mathbf{B}_{\beta\nu}\mathbf{B}^{\nu\alpha}\right], \tag{A.3f}$$

$$\mathcal{L}_{T,8} = g'^4 F_{T,8} \operatorname{tr}\left[\mathbf{B}_{\mu\nu}\mathbf{B}^{\mu\nu}\right] \operatorname{tr}\left[\mathbf{B}_{\alpha\beta}\mathbf{B}^{\alpha\beta}\right], \tag{A.3g}$$

$$\mathcal{L}_{T,9} = g'^4 F_{T,9} \operatorname{tr}\left[\mathbf{B}_{\alpha\mu}\mathbf{B}^{\mu\beta}\right] \operatorname{tr}\left[\mathbf{B}_{\beta\nu}\mathbf{B}^{\nu\alpha}\right]. \tag{A.3h}$$

References

1. M.S. Chanowitz, M.K. Gaillard, Nucl. Phys. B **261**, 379 (1985)
2. G.J. Gounaris, R. Kogerler, H. Neufeld, Phys. Rev. D **34**, 3257 (1986)
3. B.W. Lee, C. Quigg, H.B. Thacker, Phys. Rev. Lett. **38**, 883 (1977)
4. B.W. Lee, C. Quigg, H.B. Thacker, Phys. Rev. D **16**, 1519 (1977)
5. J.M. Cornwall, D.N. Levin, G. Tiktopoulos, Phys. Rev. D **10**, 1145 (1974). (Erratum: [Phys. Rev. D **11**, 972 (1975)])
6. G. Aad et al. [ATLAS Collaboration], Phys. Rev. Lett. **113**(14), 141803 (2014). arXiv:1405.6241 [hep-ex]
7. The ATLAS collaboration [ATLAS Collaboration], ATLAS-CONF-2014-013
8. CMS Collaboration [CMS Collaboration], CMS-PAS-FSQ-13-008
9. E. Accomando et al. [ECFA/DESY LC Physics Working Group Collaboration], Phys. Rept. **299**, 1 (1998). arXiv:hep-ph/9705442
10. T. Abe et al. [Linear Collider American Working Group Collaboration]. arXiv:hep-ex/0106057
11. J.F. Gunion, A. Tofighi-Niaki, Phys. Rev. D **36**, 2671 (1987)
12. A. Tofighi-Niaki, J.F. Gunion, Phys. Rev. D **38**, 1433 (1988)
13. V.D. Barger, K.M. Cheung, T. Han, R.J.N. Phillips, Phys. Rev. D **52**, 3815 (1995). arXiv:hep-ph/9501379
14. T. Han, H.J. He, C.P. Yuan, Phys. Lett. B **422**, 294 (1998). arXiv:hep-ph/9711429
15. D. Dominici, Riv. Nuovo Cim. 20N11, 1 (1997)
16. D. Dominici, Riv. Nuovo Cim. **20**, 1 (1997). arXiv:hep-ph/9711385
17. E. Boos, H.J. He, W. Kilian, A. Pukhov, C.P. Yuan, P.M. Zerwas, Phys. Rev. D **57**, 1553 (1998). arXiv:hep-ph/9708310
18. E. Boos, H.J. He, W. Kilian, A. Pukhov, C.P. Yuan, P.M. Zerwas, Phys. Rev. D **61**, 077901 (2000). arXiv:hep-ph/9908409
19. R. Chierici, S. Rosati, M. Kobel, LC-PHSM-2001-038
20. S. Rosati, PhD thesis
21. M. Beyer, W. Kilian, P. Krstonosic, K. Mönig, J. Reuter, E. Schmidt, H. Schröder, Eur. Phys. J. C **48**, 353 (2006). arXiv:hep-ph/0604048
22. S. Liebler, G. Moortgat-Pick, G. Weiglein, JHEP **1506**, 093 (2015). arXiv:1502.07970 [hep-ph]
23. A. Denner, S. Dittmaier, T. Hahn, Phys. Rev. D **56**, 117 (1997). arXiv:hep-ph/9612390
24. A. Denner, T. Hahn, Nucl. Phys. B **525**, 27 (1998). arXiv:hep-ph/9711302
25. E. Accomando, A. Denner, S. Pozzorini, JHEP **0703**, 078 (2007). arXiv:hep-ph/0611289
26. L. Linssen, A. Miyamoto, M. Stanitzki, H. Weerts. arXiv:1202.5940 [physics.ins-det]
27. P. Lebrun et al. arXiv:1209.2543 [physics.ins-det]
28. M. Aicheler et al., CERN-2012-007, SLAC-R-985, KEK-Report-2012-1, PSI-12-01, JAI-2012-001
29. H. Baer et al. arXiv:1306.6352 [hep-ph]
30. T. Behnke et al. arXiv:1306.6329 [physics.ins-det]
31. T. Appelquist, J. Carazzone, Phys. Rev. D **11**, 2856 (1975)
32. S. Weinberg, Phys. A **96**, 327 (1979)
33. H. Georgi, Ann. Rev. Nucl. Part. Sci. **43**, 209 (1993)
34. R. Contino, C. Grojean, D. Pappadopulo, R. Rattazzi, A. Thamm, JHEP **1402**, 006 (2014). arXiv:1309.7038 [hep-ph]
35. M.J.G. Veltman, Nucl. Phys. B **123**, 89 (1977)
36. P. Sikivie, L. Susskind, M.B. Voloshin, V.I. Zakharov, Nucl. Phys. B **173**, 189 (1980)
37. W. Kilian, Springer Tracts Mod. Phys. **198**, 1 (2003)
38. W. Kilian, T. Ohl, J. Reuter, M. Sekulla, Phys. Rev. D **91**, 096007 (2015). arXiv:1408.6207 [hep-ph]
39. W. Buchmüller, D. Wyler, Nucl. Phys. B **268**, 621 (1986)
40. K. Hagiwara, S. Ishihara, R. Szalapski, D. Zeppenfeld, Phys. Lett. B **283**, 353 (1992)
41. K. Hagiwara, S. Ishihara, R. Szalapski, D. Zeppenfeld, Phys. Rev. D **48**, 2182 (1993)
42. O.J.P. Eboli, M.C. Gonzalez-Garcia, J.K. Mizukoshi, Phys. Rev. D **74**, 073005 (2006). arXiv:hep-ph/0606118
43. B. Grzadkowski, M. Iskrzynski, M. Misiak, J. Rosiek, JHEP **1010**, 085 (2010). arXiv:1008.4884 [hep-ph]
44. M. Baak et al. arXiv:1310.6708 [hep-ph]
45. C. Arzt, M.B. Einhorn, J. Wudka, Nucl. Phys. B **433**, 41 (1995). doi:10.1016/0550-3213(94)00336-D. arXiv:hep-ph/9405214
46. A.C. Longhitano, Nucl. Phys. B **188**, 118 (1981)
47. T. Appelquist, G.H. Wu, Phys. Rev. D **48**, 3235 (1993). arXiv:hep-ph/9304240
48. M. Sekulla, PhD thesis, University of Siegen (2015)
49. A. Alboteanu, W. Kilian, J. Reuter, JHEP **0811**, 010 (2008). arXiv:0806.4145 [hep-ph]
50. W. Kilian, T. Ohl, J. Reuter, Eur. Phys. J. C **71**, 1742 (2011). arXiv:0708.4233 [hep-ph]

51. M. Moretti, T. Ohl, J. Reuter, In: *2nd ECFA/DESY Study 1998-2001* 1981–2009. arXiv:hep-ph/0102195
52. W. Kilian, J. Reuter, S. Schmidt, D. Wiesler, JHEP **1204**, 013 (2012). arXiv:1112.1039 [hep-ph]
53. N.D. Christensen, C. Duhr, B. Fuks, J. Reuter, C. Speckner, Eur. Phys. J. C **72**, 1990 (2012). arXiv:1010.3251 [hep-ph]
54. W. Kilian, T. Ohl, J. Reuter, C. Speckner, JHEP **1210**, 022 (2012). arXiv:1206.3700 [hep-ph]
55. B. Chokoufe Nejad, W. Kilian, J. Reuter, C. Weiss, PoS EPS - HEP2015. 317 (2015). arXiv:1510.02739 [hep-ph]
56. C. Weiss, B. Chokoufe Nejad, W. Kilian, J. Reuter, PoS EPS - HEP2015. 466 (2015). arXiv:1510.02666 [hep-ph]
57. N. Greiner, A. Guffanti, T. Reiter, J. Reuter, Phys. Rev. Lett. **107**, 102002 (2011). arXiv:1105.3624 [hep-ph]
58. T. Binoth, N. Greiner, A. Guffanti, J. Reuter, J.-P. Guillet, T. Reiter, Phys. Lett. B **685**, 293 (2010). arXiv:0910.4379 [hep-ph]
59. W. Kilian, J. Reuter, T. Robens, Eur. Phys. J. C **48**, 389 (2006). arXiv:hep-ph/0607127
60. M. Idzik [FCAL Collaboration], Acta Phys. Polon. B **46**(7), 1297 (2015)
61. J.S. Marshall, A. Münnich, M.A. Thomson, Nucl. Instrum. Methods A **700**, 153 (2013). arXiv:1209.4039 [physics.ins-det]
62. W. Kilian, T. Ohl, J. Reuter, M. Sekulla, Phys. Rev. D **93**(3), 036004 (2016). arXiv:1511.00022 [hep-ph]
63. W. Kilian, Int. J. Mod. Phys. A **15**, 2387 (2000). doi:10.1016/S0217-751X(00)00245-5